Autophagy

Volume 11 • Issue 11 • November 2015

Editor-in-Chief
Daniel J. Klionsky
University of Michigan

Taylor & Francis
Taylor & Francis Group

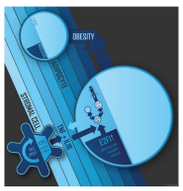

Autophagy

ISSN: 1554-8627 (Print) 1554-8635 (Online) Journal homepage: https://www.tandfonline.com/loi/kaup20

Cholesterol derivatives induce dephosphorylation of the histone deacetylases Rpd3/HDAC1 to upregulate autophagy

Wenmei Wu, Man Luo, Kang Li, Yichen Dai, Huiyu Yi, Yangjin Zhong, Yang Cao, Gianluca Tettamanti & Ling Tian

To cite this article: Wenmei Wu, Man Luo, Kang Li, Yichen Dai, Huiyu Yi, Yangjin Zhong, Yang Cao, Gianluca Tettamanti & Ling Tian (2020): Cholesterol derivatives induce dephosphorylation of the histone deacetylases Rpd3/HDAC1 to upregulate autophagy, Autophagy, DOI: 10.1080/15548627.2020.1725376

To link to this article: https://doi.org/10.1080/15548627.2020.1725376

Publisher: Taylor & Francis & Informa UK Limited, trading as Taylor & Francis Group

Journal: *Autophagy*

DOI: 10.1080/15548627.2020.1725376

Cholesterol derivatives induce dephosphorylation of the histone deacetylase Rpd3/HDAC1 to upregulate autophagy

Wenmei Wu[1,2], Man Luo[1,2], Kang Li[3], Yichen Dai[1,2], Huiyu Yi[1,2], Yangjin Zhong[1,2], Yang Cao[4,1], Gianluca Tettamanti[5], Ling Tian[1, 2,*]

[1] Guangdong Laboratory for Lingnan Modern Agriculture/Guangdong Provincial Key Laboratory of Agro-animal Genomics and Molecular Breeding, College of Animal Science, South China Agricultural University, Guangzhou 510642, China;

[2] Guangdong Provincial Sericulture and Mulberry Engineering Research Center, College of Animal Science, South China Agricultural University, Guangzhou 510642, China;

[3] Guangdong Provincial Key Laboratory of Insect Developmental Biology and Applied Technology, Institute of Insect Science and Technology, School of Life Sciences, South China Normal University, Guangzhou 510631, China;

[4] Biological Science Research Center/Chongqing Engineering and Technology Research Center for Novel Silk Materials, Southwest University, Chongqing 400716, China;

[5] Department of Biotechnology and Life Sciences, University of Insubria, Varese 21100, Italy;

[*] Correspondence to: tianling@scau.edu.cn

Abstract

Histone deacetylases (HDACs) are important for global gene expression and contribute to numerous physiological events. Deacetylase Rpd3 in yeast and its conserved homolog HDAC1 in mammals oppositely regulate autophagy; however, how Rpd3/HDAC1 is regulated to mediate autophagy remains unclear. Here, we showed autophagy occurrence in silkworm (*Bombyx mori*) required BmRpd3, wherein steroid hormone 20-hydroxyecdysone (20E) signaling regulated its protein level and nuclear localization negatively. Inhibition of MTOR led to dephosphorylation and nuclear-cytoplasmic translocation of BmRpd3/HsHDAC1. Besides, cholesterol, 20E, and 27-hydroxycholesterol could all induce massive dephosphorylation and cytoplasmic localization of BmRpd3/HsHDAC1, and thus autophagy by affecting MTORC1 activity. In addition, three phosphorylation sites (Ser392, Ser421, and Ser423) identified in BmRpd3 were conserved in HsHDAC1. Single or triple phosphorylation-site mutation attenuated the phosphorylation levels of BmRpd3/HsHDAC1, leading to their cytoplasmic localization and autophagy activation. In general, cholesterol derivatives, especially hydroxylated cholesterol, caused dephosphorylation and nucleo-cytoplasmic shuttling of BmRpd3/HsHDAC1 through inhibition of MTOR signaling to facilitate autophagy in *B. mori* and mammals. These findings improve our understandings of BmRpd3/HsHDAC1-mediated autophagy induced by cholesterol derivatives and shed light on their potential as a therapeutic target for neurodegenerative diseases and autophagy-related studies.

Abbreviations: 20E: 20-hydroxyecdysone; 27-OH: 27-hydroxycholesterol; ACTB: actin beta; AMPK: AMP-activated protein kinase; Atg: autophagy-related; BmSqstm1: *Bombyx* sequestosome 1; CQ: chloroquine; HDAC: histone deacetylase; LMNB: Lamin B1; MTOR: mechanistic target of rapamycin kinase; PE: phosphatidylethanolamine; SQSTM1/p62: sequestosome 1; TUBA1A: tubulin alpha 1a.

Keywords: Autophagy; BmRpd3/HsHDAC1; cholesterol derivatives; dephosphorylation; nucleo-cytoplasmic translocation; MTOR

Introduction

Macroautophagy/autophagy is a critical process responsible for the degradation of intracellular components, including damaged organelles, long-lived proteins, and lipids, widely conserved from yeast to mammals [1,2]. The initiation, nucleation, elongation, and maturation steps of autophagosome formation require a series of autophagy-related (Atg) proteins [2,3]. Nutrients and energy regulate the initiation of autophagosome formation via phosphorylation of the ULK1/Atg1-ATG13/Atg13 protein kinase complex through MTOR (mechanistic target of rapamycin kinase) signaling in coordination with the AMP-activated protein kinase (AMPK) pathway [1,4]. Unique to insects, the steroid hormone 20-hydroxyecdysone (20E) predominantly triggers the global expression of *Atg* genes and simultaneously inhibits MTOR signaling to induce autophagy initiation, highlighting the differential regulation of autophagy from yeast to mammals [5].

Moreover, post-translational modifications of Atg proteins, including acetylation, SUMOylation, and phosphorylation, all affect autophagy occurrence [6]. In addition to phosphorylation, acetylation of lysine sites in Atg proteins is a universal mechanism that regulates their autophagic functions. Starvation reduces acetyl coenzyme A activity and cytoplasmic acetylation level, which consequently results in the inactivation of histone acetyltransferase KAT8/hMOF/MYST1 and hence the induction of autophagy in mammals [7]. Besides, knockdown of AcCoAS/acetyl-coenzyme A synthetase in the *Drosophila* brain enhances autophagy, indicating a similar regulatory mechanism of autophagy by deacetylation in both *Drosophila* and mammals [8].

In mammals, deacetylation of ATG5, ATG7, LC3, and ATG12 by SIRT1 (sirtuin 1) and HDAC6 (histone deacetylase 6) promotes, while acetylase EP300/p300 inhibits autophagy [6,9,10]. In yeast, Atg3, Atg5, and Atg8 are acetylated in nutrient-rich conditions; however, Atg3 is further acetylated by acetylase Esa1 during starvation,

and then deletion of deacetylase *Rpd3* promotes starvation-induced autophagy [11]. Dysfunction of mammalian HDACs is associated with tumorigenesis and metastasis; mammalian HDACs are classified as I, II, III, and IV types, and class I type HDACs contribute to autophagic flux and skeletal muscle homeostasis in mice [12]. Knockout of *Hdac1* or *Hdac2*, which are members of mammalian class I type HDACs, inhibits autophagy, and accordingly, their overexpression upregulates autophagy in mouse skeletal muscle [13,14]. Therefore, there appear to be gaps in our understanding between lower and higher evolutionary-status organisms concerning the autophagic function of HDAC homologs. This discrepancy in autophagy regulation by acetylation in mammals and yeast has not been investigated in detail in other species. Their post-translational modifications regulate the activity of HDACs, and the subcellular localization of class I and II HDACs requires phosphorylation. Serine-site phosphorylation determines nucleo-cytoplasmic translocation of HDAC1 and occurs in inflammatory demyelinating lesions [15]. Two phosphorylation sites at Ser421 and Ser423 mediate the subcellular localization of HDAC1 in mice; in comparison, phosphorylation at Ser278 and Ser279 leads to the nuclear localization of HDAC5, while other HDAC homologs are not well documented [15-17].

Cholesterol is a cell membrane structural component essential for membrane fluidity and permeability, and also acts as a precursor for steroid hormones and bile acid biosynthesis [18-20]. The lack of cholesterol results in various inborn defects in humans, whereas excessive cholesterol causes a high risk of cardiovascular diseases [21]. Cholesterol is highly concentrated in the brain in its free state and participates in neural growth, regeneration, and repair [21,22]. However, high concentrations of cholesterol in the brain are usually associated with neurodegenerative diseases such as Alzheimer and Parkinson diseases [22,23]. Moreover, 27-hydroxycholesterol (27-OH), the major metabolite of cholesterol, increases SNCA/α-synuclein level in human dopaminergic neurons and the risk of Parkinson disease [23]. 20E is biosynthesized from cholesterol absorbed from food digestion in insects, and responsible for multiple physiological changes, including autophagy during larval molting and metamorphosis [24-26]. We found that the *Bombyx* histone deacetylase BmRpd3 was highly

conserved with mammalian homologs and essential for autophagy occurrence. 20E signaling induced the dephosphorylation of BmRpd3 and its nucleo-cytoplasmic shuttling to promote autophagy. Moreover, both cholesterol and 27-OH regulate the dephosphorylation of BmRpd3/HsHDAC1, which were similar to 20E by affecting MTOR activity in organisms such as *Bombyx* and mammals. These results document the role of cholesterol derivatives in BmRpd3/HsHDAC1-mediated autophagy and provide potential therapeutic targets for neurodegenerative disease.

Results

Deacetylase BmRpd3 is highly conserved and required for protein deacetylation.

The homolog of mammalian HDAC1 has not been functionally identified in *B. mori*. We found BmRpd3 by blasting the amino acid sequence of HsHDAC1 (BAG70111.1) against the *Bombyx* genome. We also performed a phylogenetic analysis of the BmRpd3 homolog between more than 30 species from *Saccharomyces cerevisiae* to *Homo sapiens*, mainly including Insecta, Crustacea, and Decapoda. Results showed that BmRpd3 was more conserved with the homologs in *Pieris rapae* and other lepidopteran species but still harbored around 80% identity compared to HsHDAC1 (**Fig. 1A**).

We further verified whether BmRpd3 possessed the catalytic activity for deacetylation using *BmRpd3* RNAi in *B. mori* larvae. After *BmRpd3* RNAi for 24 h, we observed a significant reduction of BmRpd3 protein levels; consequently, the acetylation levels of total proteins were increased in the *B. mori* larval fat body as indicated by the pan-acetyl-lysine western blot detection (**Fig. 1B**). Conversely, overexpression of *BmRpd3* decreased the acetylation levels of total protein in *Bombyx* BmN cells (**Fig. 1B'**). Thus, BmRpd3 was identified as a functional deacetylase to mediate protein deacetylation in *B. mori*.

***BmRpd3 is indispensable for autophagy in* B. mori.**

Deletion of HDAC1 reduces autophagy, and its overexpression upregulates autophagy in mice [12]. Thus, we investigated the involvement of BmRpd3 in autophagy in *B. mori*. RNAi knockdown experiments showed that the transcriptional and protein levels of BmRpd3 in the *B. mori* fat body were reduced by approximately 50% at 24 h after *BmRpd3* RNAi treatment (**Fig. 2A and B**). The protein levels of autophagic substrate *Bombyx* sequestosome 1 (BmSqstm1) accumulated and, conversely, inhibited BmAtg8–phosphatidylethanolamine (PE) formation, indicating an autophagy block after *BmRpd3* RNAi treatment (**Fig. 2B and B'**). Immunofluorescent staining of BmRpd3 indicated that the protein expression reduced both in the nucleus and cytoplasm after RNAi treatment. Moreover, BmAtg8 was mainly arrested in the nucleus after *BmRpd3* RNAi, followed by a decrease of BmAtg8 puncta in the cytoplasm (**Fig. 2C and C'**).

In contrast, the BmSqstm1 protein level decreased, while BmAtg8–PE conjugation and co-overexpressed FLAG-BmAtg8–PE formation increased in BmN cells overexpressing *BmRpd3*, showing a direct promotion of autophagy by BmRpd3 (**Fig. 2D-E'**). Moreover, EGFP-BmAtg8 puncta and LysoTracker Red staining were induced in cells overexpressing *BmRpd3*, which was consistent with autophagy occurrence as indicated by BmSqstm1 degradation and BmAtg8–PE formation (**Fig. 2F-G'**). These results show that autophagy requires BmRpd3 occurrence in *Bombyx*.

BmRpd3 protein levels and nuclear localization are negatively related by 20E during larval-pupal metamorphosis.

The fat body is a key site for material storage or utilization and insect innate immunity, and 20E regulates multiple physiological processes in this tissue [27,28]. Developmental profiles showed that BmRpd3 protein levels attenuated in the *B. mori* fat body from day 2 of the 5th instar (5L-2) to day 2 of the prepupa (PP2), which was inversely proportional to 20E titer (**Fig. 3A and A'**). Immunofluorescent staining of BmRpd3 co-stained with DAPI indicated that BmRpd3 almost completely localized in

the nuclei of the fat body during larval feeding stage; however, it shuttled from the nucleus to the cytoplasm at wandering (W), PP1, and PP2 stages (**Fig. 3B and B'**), similar to the mammalian HDAC1 that also presents nucleo-cytoplasmic shuttling [15-17]. Overall, BmRpd3 is a nuclear-localized protein that is negatively associated with 20E titer in the hemolymph during larval-pupal metamorphosis.

20E signaling induces BmRpd3 nucleo-cytoplasmic translocation and autophagy in B. mori.

According to the developmental profiles, 20E is implicated in the negative regulation of BmRpd3 protein levels and its nuclear localization (**Fig. 3**). Thus, we investigated the regulatory mechanism of 20E on BmRpd3 further. Three-dimensional structure analysis revealed that there were high binding affinities and close interactions between 20E, cholesterol, 27-OH, and BmRpd3/HsHDAC1 (**Fig. S1A-B"**). We injected 20E into 5L-3 larvae at a low titer when BmRpd3 mainly localized in the nucleus [4,27]. *BmE75a* is the primary response gene of 20E, and its mRNA levels increased > 10-fold in the fat body at 24 h after 20E injection. Subsequently, BmSqstm1 and BmRpd3 protein levels decreased, whereas BmAtg8–PE conjugation was promoted (**Fig. 4A**, **A' and S2A**), and then BmRpd3 was shuttled from the nucleus to the cytoplasm in the fat body (**Fig. 4A" and A'"**). Moreover, BmSqstm1 and the overexpressed BmRpd3-HA protein levels decreased, while BmAtg8–PE formation and nucleo-cytoplasmic translocation of BmRpd3-HA were enhanced by 20E treatment in BmN cells (**Fig. 4B-B'" and S2B**).

20E signaling transduction occurs through its heterodimer EcR/USP complex [4,27]. RNAi-mediated knockdown of *BmUsp* significantly downregulated *BmUsp* mRNA levels in the *Bombyx* fat body (**Fig. 4C**). In contrast to 20E treatment, *BmUsp* RNAi caused accumulation of BmSqstm1, BmRpd3, and full-length BmAtg8, as well as a decrease in BmAtg8–PE formation (**Fig. 4C' and S2C**). In addition, fluorescent BmRpd3 decreased in the cytoplasm after *BmUsp* RNAi treatment (**Fig. 4C" and C'"**). These results suggest that 20E regulates autophagy occurrence by affecting

BmRpd3 in *B. mori*.

Although 20E signaling induced nuclear export and consequent degradation of BmRpd3 protein, the mechanisms of these processes remain unclear. As predicted by GPS-SUMO software, BmRpd3 may undergo SUMOylation modification (**Table S1**). An antibody against SUMOylation detected that the immunoprecipitated BmRpd3 was SUMOylated 6 h after 20E treatment in BmN cells (**Fig. S2D**). Overall, 20E signaling induces the nuclear export and degradation of BmRpd3 in *B. mori*.

Cholesterol promotes the nuclear export of BmRpd3 and autophagy.

Cholesterol is the precursor of 20E, and then we investigated whether cholesterol regulated the subcellular localization of BmRpd3. The degradation of BmSqstm1 and the increase of BmAtg8–PE conjugation indicated that autophagy was induced 24 h after cholesterol treatment in *Bombyx* fat body (**Fig. S3A and A'**). Immunofluorescent staining revealed that the nucleo-cytoplasmic shuttling of BmRpd3 occurred 12 h and 24 h after cholesterol treatment (**Fig. S3A' and B**). Moreover, BmSqstm1 and BmRpd3 protein levels decreased, whereas BmAtg8–PE formation increased after overexpression of *BmRpd3* for 48 h and then treated with different doses of cholesterol (10 to 500 μM) (**Fig. S3C and C'**). In addition, immunofluorescent staining indicated that the overexpressed BmRpd3-HA exported from the nucleus to the cytoplasm after treatment with different doses of cholesterol (**Fig. S3D and D'**). In general, cholesterol-induced nucleo-cytoplasmic translocation of BmRpd3 and autophagy are similar to that of insect molting hormone 20E in *B. mori*.

Ser392, Ser421, and Ser423 mediate the phosphorylation, nuclear export, and autophagic function of BmRpd3.

Phosphorylation mediates the subcellular localization of HDAC5 and HDAC1 in mammals [15,17]; therefore, we next investigated whether BmRpd3 exhibited phosphorylation modification. Three phosphorylation sites, Ser392, Ser421, and

Ser423, were identified in BmRpd3-HA by liquid chromatography-mass spectrometry (LC-MS). These serine residues were conserved from insects to humans but not in *C. elegans* and *S. cerevisiae* (**Fig. S4A-C**). Single phosphorylation-site mutations significantly affected BmRpd3-HA phosphorylation, and triple phosphorylation-site mutation abolished phosphorylation of BmRpd3-HA as detected using an antibody against phosphoserine/threonine/tyrosine-phosphorylation, and led to its cytoplasmic localization (**Fig. 5A-B'**). Moreover, BmRpd3 completely distributed in the cytoplasm after the triple phosphorylation-site mutation (**Fig. 5C**).

Phosphorylation modification also regulated the autophagic function of BmRpd3. BmSqstm1 protein became significantly degraded, while EGFP-BmAtg8–PE formation was induced by the overexpression of single or triple phosphorylation-site mutation in *BmRpd3* under nutrient-rich conditions, which became further enhanced after 20E treatment (**Fig. 6A and S2G**). Accordingly, overexpression of phosphorylation-site mutants, especially the triple phosphorylation-site mutated *BmRpd3* induced EGFP-BmAtg8 puncta in the cytoplasm, which was further promoted by 20E addition (**Fig. 6B and B'**). Overall, dephosphorylation at Ser392, Ser421, and Ser423 residues in BmRpd3 causes its nucleo-cytoplasmic translocation and promotes autophagy in *B. mori*.

Cholesterol derivatives inhibit MTOR signaling to dephosphorylate BmRpd3.

Similar to cholesterol, 20E treatment led to the dephosphorylation of immunoprecipitated BmRpd3-HA from BmN cells (**Fig. 5D and S3E**). We observed that 20E increased the cytoplasmic and decreased the nuclear BmRpd3 protein levels compared to the untreated controls (**Fig. 5E**), indicating the essential role of 20E in regulating the nucleo-cytoplasmic translocation of BmRpd3 via dephosphorylation modification. To address how 20E interacts with signaling pathways that regulate the phosphorylation status of BmRpd3, we individually injected 20E, the AMPK-specific activator metformin, the MTORC1-specific inhibitor rapamycin, and the AMPK-specific inhibitor compound C into 5L-3 larvae. Both 20E and rapamycin

treatments led to a significant decrease in BmRpd3 protein and induced its cytoplasmic localization in the fat body (**Fig. S2E-F**). Furthermore, the phosphorylation levels and nuclear localization of BmRpd3-HA attenuated after 20E and rapamycin treatments in BmN cells (**Fig. 5F-G'**). We then investigated whether the derivatives of cholesterol interacted with MTOR signaling and found that 20E, cholesterol, and 27-OH treatment all inhibited nutrient signaling, indicated by changes in p-EIF4EBP1 levels (**Fig. 7A-C'**). Moreover, *BmMTORC1* RNAi decreased the phosphorylation levels and nuclear localization of BmRpd3-HA, suggesting cooperation between 20E and MTOR signaling in regulating the phosphorylation modification of BmRpd3 (**Fig. 7D-F**).

Cholesterol, 20E, and 27-OH administration results in the dephosphorylation and nuclear export of HsHDAC1 and then promotes autophagy.

We next investigated whether cholesterol, 20E, and 27-OH could similarly regulate the phosphorylation and subcellular localization of mammalian HDAC1. As indicated by a decrease in human SQSTM1/p62 protein levels, and an increase in LC3-II formation, *HsHDAC1* overexpression in HEK 293 cells significantly induced autophagy (**Fig. 8A and S5A**). Chloroquine (CQ) treatment inhibits the fusion between autophagosome and lysosome, thus determining inhibition of the autophagic flux [1]. Also, we detected that CQ inhibited *HsHDAC1*-induced autophagic flux. Firstly, SQSTM1/p62 and LC3-II protein levels linearly accumulated in response to an increasing dose of CQ (20, 40, 60, 80 μM) in HEK 293 cells. We used 40 μM CQ for subsequent experiments (**Fig. S4D and D'**). After *HsHDAC1* overexpression and treatment with 40 μM CQ, the SQSTM1/p62 and LC3-II protein levels all significantly increased compared to *HsHDAC1* overexpression, showing inhibition of *HsHDAC1*-induced autophagic flux by CQ treatment (**Fig. 8A**). Moreover, *HsHDAC1* overexpression also induced the presence of EGFP-LC3 puncta, further indicating autophagy induction (**Fig. 8A' and A"**). Notably, degradation of both human SQSTM1/p62 and overexpressed HsHDAC1-HA, and LC3-II formation were induced

6 h after 250 μM cholesterol treatment; in contrast, they were all accumulated after 40 μM CQ addition (**Fig. 8B and S5B**). Besides, the phosphorylation levels and nuclear localization of overexpressed HsHDAC1-HA simultaneously and significantly decreased after cholesterol treatment (**Fig. 8B', B" and S5C**).

We hypothesized that 20E would have a similar function as cholesterol in regulating HsHDAC1 in HEK 293 cells. The results showed that 5 μM 20E was able to induce autophagic flux as well as dephosphorylation and nucleo-cytoplasmic translocation of HsHDAC1 (**Fig. 8C-C", S5D and S5E**). Treatment with 10 μM 27-OH had similar effects compared to 20E and cholesterol treatment, demonstrating a conserved regulatory mechanism of 27-OH on HsHDAC1 dephosphorylation and autophagy (**Fig. 8D-D", S5F and S5G**). Overall, both cholesterol and its hydroxylated derivatives are able to induce dephosphorylation and nucleo-cytoplasmic shuttling of BmRpd3/HsHDAC1, and then autophagy.

BmRpd3 phosphorylation sites are functionally conserved in the regulation of HsHDAC1 phosphorylation and subcellular localization.

As the three phosphorylation sites (Ser392, Ser421, and Ser423) were conserved in BmRpd3 and HsHDAC1, we asked if these sites were involved in HsHDAC1 phosphorylation regulation. Results showed that single phosphorylation-site mutation partly attenuated, while triple phosphorylation-site mutation completely impaired phosphorylation of HsHDAC1 and led to the linear decrease of its nuclear localization (**Fig. 9A-A"**). Autophagy was gradually induced after the overexpression of the single and triple phosphorylation-site mutated *HsHDAC1*, as shown by SQSTM1/p62 and LC3-II protein levels, enhanced further by 27-OH treatment (**Fig. 9B and B'**). Moreover, triple phosphorylation-site mutation of HsHDAC1-HA induced the formation of mCherry-LC3 puncta, which was further promoted by 27-OH treatment (**Fig. S5H and H'**). Overall, the phosphorylation sites identified on BmRpd3 are functionally conserved in *Bombyx* and humans and mediate the phosphorylation and nuclear localization of its mammalian homolog HsHDAC1.

Cholesterol derivatives regulate the phosphorylation of HsHDAC1 through their interaction with HsMTORC1 signaling.

Similar to BmMTORC1, the HsMTORC1 was hypothesized to regulate the phosphorylation of HsHDAC1. As expected, treatments with 27-OH and rapamycin both reduced HsHDAC1 phosphorylation levels and nuclear localization in HEK 293 cells (**Fig. 9C-C"**). Cholesterol, 20E, and 27-OH treatments all led to the inhibition of HsMTORC1 activity as indicated by a decrease of p-EIF4EBP1 protein levels (**Fig. 10A-C'**). In HEK 293 cells, *HsMTORC1* RNAi significantly reduced *HsMTORC1* transcripts after 48 h, and then the phosphorylation of HsHDAC1-HA was almost abolished, which consequently led to the nucleo-cytoplasmic translocation of fluorescent HsHDAC1-HA (**Fig. 10D-F**). In conclusion, cholesterol derivatives are functionally conserved and are able to dephosphorylate BmRpd3/HsHDAC1 through the inhibition of MTORC1 activity, leading to the cytoplasmic localization of BmRpd3/HsHDAC1, and thus promoting autophagy (**Fig. 11**).

Discussion

Oxysterols exhibit an effective and evolutionarily conserved ability to regulate Rpd3/HDAC1 function in* B. mori *and humans.

Members of class I HDACs in mammals promote autophagy, whereas Rpd3, the homolog of HsHDAC1 in yeast, inhibits autophagy induction that is not documented in other species [11,12]. Knockdown of AcCoAS/acetyl-coenzyme A synthetase in the *Drosophila* brain enhances autophagy, which is consistent with the induction of autophagy by the reduction of acetyl coenzyme A activity and cytoplasmic acetylation levels in mammals [7,8]. In the present study, we demonstrate that HsHDAC1 and its homolog BmRpd3 in *B. mori* could deacetylate proteins and are required for autophagy occurrence. Their similar functions imply that the regulatory mechanism of

BmRpd3/HsHDAC1 is likely highly conserved in *Bombyx* and humans, and potentially, from insects to mammals.

It is well known that cholesterol has a close relationship with deacetylases involved in the regulation of cholesterol biosynthesis and catabolism [21,29]. However, whether the cholesterol and its derivatives inversely regulate the functions of deacetylases remains unclear. Cholesterol induces autophagic and apoptotic features in mammalian insulin-secreting βTC-6 and INS-1 cells, although the precise mechanism of this regulation is not well defined [30]. Here we show that cholesterol and oxysterols such as 20E and 27-OH are all able to induce the dephosphorylation of BmRpd3/HDAC1 homologs, as well as their cytoplasmic localization through inactivation of MTORC1 signaling, revealing a conserved regulation of HsHDAC1 homologs by cholesterol and oxysterol (**Fig. 5, 7, 9, and 10**). Notably, oxysterols that freely pass through the blood-brain barrier are more efficient at inducing dephosphorylation and nucleo-cytoplasmic translocation of BmRpd3/HDAC1 and autophagy, indicating that the hydroxylated metabolites of cholesterol may play more important roles in some physiological processes.

Oxysterols are involved in several events underlying Alzheimer pathogenesis. Certain oxysterols cause neuron dysfunction and degeneration; conversely, some display neuroprotective effects. 24-hydroxylcholesterol increases the transcription and translation of the deacetylase SIRT1, which prevents the neurotoxic accumulation of the hyperphosphorylated tau protein [31]. However, 27-OH decreases the proteasomal degradation of SNCA and results in memory deficits and synucleinopathy risk [23]. Whether class I type HDACs have similar functions to class II type SIRTs in neurodegenerative diseases and whether other oxysterols functionally differ from 24-hydroxycholesterol in nervous diseases are worthy of investigation.

***20E regulates autophagy occurrence via multiple pathways in* B. mori.**

In insects, 20E signaling controls programmed cell death, mainly including autophagy and apoptosis [4,32,33]. 20E upregulates autophagy occurrence via multiple pathways;

several studies have shown that 20E induces massive autophagy during larval-pupal metamorphosis through EcR-USP signaling by upregulating the expression of *Atg* genes in *Drosophila* and *Bombyx* [4,6]. Moreover, 20E interacts with the nutrient pathway to inhibit the activity of BmMTORC1 and initiate the formation of autophagosomes through the phosphorylation of the Atg1-Atg13 protein complex [4]. Besides, 20E signaling upregulates the transcription of most genes encoding subunits of the vacuolar-type H+-adenosine triphosphatases (BmV-ATPases) from V_0 and V_1 subcomplexes and the subunit assembly in *B. mori*, mainly through the inhibition of BmMTORC1 activity and induction of BmTFEB (*Bombyx* transcription factor EB) transcription and nuclear translocalization [34]. In addition, 20E also induces starvation-like conditions in *Bombyx* by reducing food consumption [26,35].

Herein, we describe that BmMTOR1 signaling mediates BmRpd3 phosphorylation and nuclear localization; whereas, 20E inhibits BmMTORC1 signaling and then dephosphorylates BmRpd3, resulting in its nucleo-cytoplasmic translocation and consequent promotion of autophagy (**Fig. 11**). Notably, 20E signaling simultaneously induced SUMOylation and degradation of BmRpd3, although the function and mechanism of this process are still unclear.

Materials and methods

Animals and cell culture.

Silkworms (Dazao) were provided by the Sericultural and Agri-Food Research Institute of the Guangdong Academy of Agricultural Sciences (Guangzhou, China). Insects were reared on fresh mulberry leaves in the laboratory at 25°C under a 14 h light/10 h dark cycle [34,36].

BmN cells were maintained in Grace's insect medium (Sigma-Aldrich, G9771) supplemented with 10% fetal bovine serum; Human HEK 293 cells (ATCC, CRL-1573™) were cultured in Dulbecco's Modified Eagle Medium (ThermoFisher, 10569044) supplemented with 5% fetal bovine serum (AusGeneX, FBS500-S).

Plasmid construction and transfection.

BmRpd3 (XM_028180486.1) cDNAs were cloned from *B. mori* total cDNA and inserted into the pIEx4 overexpression vector fused with HA tag [27,34]. *HsHDAC1* was inserted into the pCMV3 overexpression vector (Sino Biological, HG11486-CY). *BmRpd3* and *HsHDAC1* were mutated accordingly. BmN (ATCC, CRL-8910™) or HEK 293 cells were transfected with *BmRpd3*- or *HsHDAC1*-containing plasmids using the FuGENE® HD Transfection Reagent (Promega, E2311) or TransIntro™ EL Transfection Reagent (TransGen Biotech, FT201-01) according to the manufacturer's instructions.

Chemical treatments.

Metformin (Selleck, S1950; 30 μg/larva), rapamycin (Selleck ,S1039; 10 μg/larva), compound C (Sigma-Aldrich, P5499; 5 μg/larva), 20E (Sigma-Aldrich, H5142; 5 μg/larva) and cholesterol (Yuanye Biology, 57885; 8 μg/larva) were individually injected into silkworm larva. Control groups were injected with the same volume of solvent [4,34]. Metformin (5 μM), rapamycin (10 μM), compound C (10 μM), cholesterol (5, 10, 100, 250 or 500 μM) and 20E (5 μM) were used in BmN cells; cholesterol (250 μM), 20E (5 μM) and 27-OH (Yuanye Biology, B21770; 10 μM) were used in HEK 293 cells. Different concentrations of CQ (Sigma-Aldrich, C6628; 20, 40, 60 or 80 μM) were added to HEK 293 cells for 3 h. Ten animals were included in each group, and three biological replicates were performed.

RNAi.

The double-stranded RNA (dsRNA) of *BmRpd3* and *egfp* were generated using T7 RiboMAX™ Express RNAi system (Promega, P1700) according to the manufacturer's instruction. Each larva was injected with *BmRpd3* dsRNA (50 μg) at

12 h before initiation of wandering (IW), and *egfp* dsRNA (50 μg) was injected as a control. *BmMTORC1* and *HsMTORC1* siRNA were synthesized (Sangon Biotech) and transfected into BmN or HEK 293 cells for 48 h, *egfp* siRNA transfection was used as the negative control. All primers used in this paper are listed in Table S2.

Quantitative real-time PCR (qPCR).

Total RNA from fat body tissue and cells was extracted using TRIzol reagent (TaKaRa, RR037A), and cDNA was generated using the PrimeScript™ RT reagent Kit (TaKaRa, RR047A). qPCR was performed as previously described [36]. The *BmRp49* and *ACTB* genes were used as the reference genes.

Immunoprecipitation and western blot.

BmN cells overexpressing different forms of *BmRpd3-HA* and HEK 293 cells overexpressing different forms of *HsHDAC-HA* were harvested and lysed in Nonidet P-40 lysis buffer (Beyotime Biotechnology Co., Ltd., P0013F) supplemented with a protease inhibitor cocktail (ThermoFisher Scientific, 78429). The supernatant of lysed cells was pre-incubated with an HA antibody (Santa Cruz Biotechnology, sc-7392; 1:200) at 4°C for 2 h. Then, the mixtures were incubated with agarose beads (Thermo Fisher Scientific, 20421) at 4°C overnight according to a standard immunoprecipitation procedure.

Western blot was performed according to the standard procedure using antibodies against BmRpd3/HsHDAC1 (Bioss, bs-1414R; 1:1000), HA (Beijing Biodragon, B1021; 1:2000), SQSTM1/p62 (Cell Signaling Technology, 5114; 1:1000), LC3B (Abcam, ab192890; 1:2000), LMNB/Lamin B1 (Bioworld, AP6001; 1:5000), BmAtg8 (1:3000) [4,34], phosphoserine/threonine/tyrosine (Abcam, ab15556; 1:2000), acetylated-lysine (Cell Signaling Technology, 9441; 1:1000), p-EIF4EBP1-T37/46 (ABclonal Technology, AP0030; 1:1000), SUMOylation (PTM Biolabs, PTM-1110; 1:2000), and BmSqstm1 (ABclonal Technology, A18679;

1:3000). TUBA1A/tubulin alpha 1a (Beyotime Biotechnology Co., Ltd, AT819; 1:5000) and ACTB/actin beta (ProMab, 20270; 1:1000) were used as the reference proteins. Images of western blots were taken under a series of exposure time, and the moderately exposed blots without over-saturation were used for quantification and figure presentation. ImageJ software (National Institutes of Health, USA) was used to quantify the protein blots. Three independent biological replicates were performed.

Isolation of nuclear and cytoplasmic proteins.

BmN cells were treated with 5 μM 20E for 6 h, or overexpressed with wild type or triple phosphorylation-site mutated *BmRpd3-HA*. Cells were then harvested for nuclear and cytoplasmic extraction using a NE-PERTM Nuclear Cytoplasmic Extraction Reagent Kit (Pierce, 78833) according to the manufacturer's instruction. The separated proteins were evaluated with western blots.

Immunofluorescent staining.

The perivisceral fat body and cells were collected for immunofluorescent staining with BmRpd3 or HA tag primary antibodies (Santa Cruz Biotechnology, sc-7392 ; 1:200), then further co-stained with DAPI (Beyotime Biotechnology Co., Ltd, C1005) as previously described [4,36]. Fluorescence observation was conducted under a confocal microscope equipped with an Olympus digital camera (Olympus FV3000, Tokyo). To quantify Alexa Fluor 488-labeled BmRpd3, BmRpd3-HA, HsDAC1-HA, or GFP-LC3/BmAtg8 puncta, 150-200 fat body cells or a total of 30 overexpressed BmN cells from three independent biological repeats were recorded and analyzed using ImageJ software.

LysoTracker staining.

Sterilized coverslips were placed in 6-well plates (Guangzhou Jet Bio-Filtration Co.,

Ltd, TCP-010-006) during cell plating. After pre-incubated for 24 h, the BmN cells were transfected with pIEx-4-BmRpd3-HA for 12, 24, and 36 h before being stained with LysoTracker Red DND-99 (Thermo Fisher Scientific, L7528) [4]. Observation was performed under an Olympus FV300 confocal microscope.

LC-MS/MS.

The phosphorylation sites of immunoprecipitated BmRpd3 were determined by matrix-assisted laser desorption ionization time-of-flight mass spectrometry using LC-MS (Applied Biosystems, Foster City). Gel-digested BmRpd3 protein was loaded onto a reversed-phase analytical column (75 μm i.d. × 150 mm, packed with Acclaim PepMap RSLC C18, ThermoFisher; 2 μm, 100Å, nanoViper) and separated by a gradient elution buffer. The MS analysis of peptides was performed on a Q Exactive hybrid quadrupole-Orbitrap mass spectrometer (ThermoFisher, USA). Protein identification was performed with MASCOT software (Mascot SoftWeb Solution Pvt. Ltd., Uttarakhand) by searching Uniprot for *B. mori*.

Bioinformatics analysis.

Phylogenetic analysis was constructed using the MEGA7.0 software (Molecular Evolutionary Genetics Anlysis, USA) and the Neighbor-Joining method. Only values > 50% were indicated. The three-dimensional structure between BmRpd3/HsHDAC1 and cholesterol derivatives was generated using AutoDock Tool software (The Scripps Research Institute, USA).

Statistical analysis.

Experimental data were analyzed by Student's *t*-test, *$p < 0.05$; **$p < 0.01$; ***$p < 0.001$. Values are presented as the means ± standard deviation of three independent biological replicates.

Acknowledgements

This study was supported by the National Science Foundation of China to LT (NSFC; 31672368, 31970463), the Natural Science Foundation of Guangdong Province to LT (2017A030311024), and NSFC to KL (31702053).

Disclosure

The authors have no conflicts of interest.

References:

[1] Klionsky DJ, Abdelmohsen K, Abe A, et al. Guidelines for the use and interpretation of assays for monitoring autophagy (3rd edition). Autophagy. 2016; 12(1): 1–222.

[2] Lee CY, Cooksey BA, Baehrecke EH. Steroid regulation of midgut cell death during *Drosophila* development. Dev Bio. 2002; 250 (1): 101-111.

[3] He C, Klionsky DJ. Regulation mechanisms and signaling pathways of autophagy. Annu Rev Genet. 2009; 43: 67-93.

[4] Tian L, Ma L, Guo EE, et al. 20-Hydroxyecdysone upregulates *Atg* genes to induce autophagy in the *Bombyx* fat body. Autophagy. 2013; 9(8): 1172-1187.

[5] Chang YY, Neufeld TP. Autophagy takes flight in *Drosophila*. FFBS Letters. 2010; 584 (7): 1342-1349.

[6] Popelka H, Klionsky DJ. Post-translationally-modified structures in the autophagy machinery: an integrative perspective. FEBS J. 2015; 282(18): 3474-3488.

[7] Marino G, Niso-Santano M, Baehrecke EH, et al. Self-consumption: the interplay of autophagy and apoptosis. Nat Rev Mol Cell Biol. 2014; 15 (2): 81-94.

[8] Eisenberg T, Schroeder S, Buttner S, et al. A histone point mutation that switches on autophagy. Autophagy. 2014; 10(6): 1143-1145.

[9] Huang R, Xu Y, Wan W, et al. Deacetylation of nuclear LC3 drives autophagy initiation under starvation. Mol Cell. 2015; 57(3): 456-466.

[10] Lee IH, Finkel T. Regulation of autophagy by the p300 acetyltransferase. J Biol Chem . 2009; 284(10): 6322-6328.

[11] Yi C, Ma M, Ran L, et al. Function and molecular mechanism of acetylation in autophagy regulation. Science. 2012; 336(6080): 474-477.

[12] Moresi V, Carrer M, Grueter CE, et al. Histone deacetylases 1 and 2 regulate autophagy flux and skeletal muscle homeostasis in mice. Proc Natl Acad Sci U S A. 2012; 109(5): 1649-1654.

[13] Kim J, Kundu M, Viollet B, et al. AMPK and mTOR regulate autophagy through direct phosphorylation of Ulk1. Nat Cell Biol. 2011; 13(2): 132-141.

[14] Haberland M, Montgomery RL, Olson EN. The many roles of histone deacetylases in development and physiology: implications for disease and therapy. Nat Rev Genet. 2009; 10(1): 32-42.

[15] Zhu Y, Vidaurre OG, Adula KP, et al. Subcellular distribution of HDAC1 in neurotoxic conditions is dependent on serine phosphorylation. J Neurosci. 2017; 37(31): 7547-7559.

[16] Greco TM, Yu F, Guise AJ, et al. Nuclear import of histone deacetylase 5 by requisite nuclear localization signal phosphorylation. Mol Cell Proteomics. 2011; 10(2): M110.004317.

[17] Gregoretti IV, Lee YM, Goodson HV. Molecular evolution of the histone deacetylase family: functional implications of phylogenetic analysis. J Mol Biol. 2004; 338(1): 17-31.

[18] Chang TY, Chang CC, Ohgami N, et al. Cholesterol sensing, trafficking, and esterification. Annu Rev Cell Dev Biol. 2006; 22: 129-157.

[19] Lingwood D, Simons K. Lipid rafts as a membrane-organizing principle. Science. 2010; 327(5961): 46-50.

[20] Head BP, Patel HH, Insel PA. Interaction of membrane/lipid rafts with the cytoskeleton: impact on signaling and function: membrane/lipid rafts, mediators of cytoskeletal arrangement and cell signaling. Biochim Biophys Acta. 2014; 1838(2): 532-545.

[21] Kirkegaard P, Edwards A, Risor MB, et al. Risk of cardiovascular disease? A

qualitative study of risk interpretation among patients with high cholesterol. BMC Fam Pract. 2013;14: 137.

[22] Kwiterovich PJ, Chen SC, Virgil DG, et al. Response of obligate heterozygotes for phytosterolemia to a low-fat diet and to a plant sterol ester dietary challenge. J Lipid Res. 2003; 44(6): 1143-1155.

[23] Schommer J, Marwarha G, Schommer T, et al. 27-Hydroxycholesterol increases alpha-synuclein protein levels through proteasomal inhibition in human dopaminergic neurons. BMC Neurosci. 2018; 19(1): 17.

[24] Gilbert LI, Rybczynski R, Warren JT. Control and biochemical nature of the ecdysteroidogenic pathway. Annu Rev Entomo. 2002; 47: 883-916.

[25] Tettamanti G, Casartelli M. Cell death during complete metamorphosis. Philos Trans R Soc Lond B Biol Sci. 2019; 374(1783): 20190065.

[26] Ryoo HD, Baehrecke EH. Distinct death mechanisms in *Drosophila* development. Curr Opin Cell Biol. 2010; 22(6): 889-895.

[27] Li K, Guo E, Hossain MS, et al. *Bombyx* E75 isoforms display stage- and tissue-specific responses to 20-hydroxyecdysone. Sci Rep. 2015; 5: 12114.

[28] Li S, Yu X, Feng Q. Fat body biology in the last decade. Annu Rev Entomol. 2019; 64: 315-333.

[29] Pipalia NH, Subramanian K, Mao S, et al. Histone deacetylase inhibitors correct the cholesterol storage defect in most Niemann-Pick C1 mutant cells. J Lipid Res. 2017; 58(4): 695-708.

[30] Wu J, Kong F, Pan Q, et al. Autophagy protects against cholesterol-induced apoptosis in pancreatic beta-cells. Biochem Biophys Res Commun. 2017; 482 (4): 678-685.

[31] Testa G, Staurenghi E, Giannelli S, et al. A silver lining for 24-hydroxycholesterol in Alzheimer's disease: The involvement of the neuroprotective enzyme sirtuin 1. Redox Bio. 2018; 17: 423-431.

[32] Xie K, Tian L, Guo XY, et al. BmATG5 and BmATG6 mediate apoptosis following autophagy induced by 20-hydroxyecdysone or starvation. Autophagy. 2016; 12(2): 381-396.

[33] Romanelli D, Casartelli M, Cappellozza S, et al. Roles and regulation of autophagy and apoptosis in the remodelling of the lepidopteran midgut epithelium during metamorphosis. Sci Rep. 2016; 6: 32939.

[34] Dai YC, Li K, Wu WM, et al. Steroid hormone 20-hydroxyecdysone induces the transcription and complex assembly of V-ATPases to facilitate autophagy in *Bombyx mori*. Insect Biochem Mol Biol. 2019; 116:103255.

[35] Wang S, Liu S, Liu H, et al. 20-hydroxyecdysone reduces insect food consumption resulting in fat body lipolysis during molting and pupation. J Mol Biol. 2010; 2(3): 128-138.

[36] Guo SY, Wu WM, Li SY, et al. 20-Hydroxyecdysone-upregulated proteases involved in *Bombyx* larval fat body destruction. Insect Mol Biol. 2018; 27(6): 724-738.

Figure legends

Figure 1. Phylogenetic analysis of the HDAC1 homologs and functional analysis of BmRpd3. (**A**) The phylogenetic tree of HDAC1 homologs constructed from 32 species, numbers indicate bootstrap value. (**B-B'**) Acetylation levels of total proteins at 24 h after *BmRpd3* RNAi treatment in *B. mori* fat body (**B**) and at 48 h after *BmRpd3-HA* overexpression in BmN cells (**B'**).

Figure 2. BmRpd3 is indispensable for autophagy in *Bombyx*. (**A-C'**) mRNA levels of *BmRpd3* (**A**), protein levels of BmSqstm1, BmAtg8, and BmRpd3 (**B**), immunofluorescent staining of BmRpd3 and BmAtg8 (**C**) at 24 h after *BmRpd3* RNAi treatment in the fat body. Quantification of BmAtg8–PE in **B** (**B'**); quantification of fluorescent BmRpd3 and BmAtg8 in **C** (**C'**). Black columns: BmRpd3; gray columns: BmAtg8–PE; wireframes indicate the magnified fields. (**D-D'**) Protein levels of BmSqstm1, BmAtg8, and BmRpd3-HA after *BmRpd3-HA* overexpression for 48 h (**D**). Quantification of BmAtg8–PE in **D** (**D'**), *egfp* overexpression is used as the control. (**E-E'**) Protein levels of BmSqstm1, FLAG-BmAtg8, and BmRpd3-HA after co-overexpression of *BmRpd3* and *FLAG-BmAtg8* for 48 h (**E**). Quantification of FLAG-BmAtg8–PE in **E** (**E'**). (**F-F'**) Punctation of EGFP-BmAtg8 in *BmRpd3* overexpressing cells, *mCherry* overexpression was used as the control (**F**). Quantification of BmAtg8 puncta in **F** (**F'**). Arrows: the typically treated cells; E-BmAtg8: EGFP-BmAtg8. (**G-G'**) LysoTracker Red staining after overexpression of *egfp-BmRpd3* compared to the *egfp*-overexpressed control (**G**). Quantification of LysoTracker Red staining in **G** (**G'**), E-BmRpd3: EGFP-BmRpd3; Lyso: LysoTracker Red staining.

Figure 3. Developmental profiles of BmRpd3 protein levels and subcellular localization in the fat body. (**A-A'**) Protein levels of BmRpd3 from 5L-2 to PP2. EW: early wandering stage; LW: late wandering stage; PP1: day 1 of the prepupa (**A**). Quantification of BmRpd3 compared to the TUBA1A in **A** (**A'**). (**B-B'**) Immunofluorescent staining of BmRpd3 from 5L-2 to PP2 (**B**). Quantification of the

total (columns) and nuclear/cytoplasmic (line chart) BmRpd3 in **B** (**B'**). N: nucleus, C: cytoplasm, and arrows indicate the typical cell with BmRpd3 localized in the cytoplasm.

Figure 4. 20E signaling induces nucleo-cytoplasmic translocation of BmRpd3 and autophagy in *Bombyx*. (**A-A'''**) mRNA levels of *BmE75a* (**A**); protein levels of BmSqstm1, BmRpd3, and BmAtg8 (**A'**); immunofluorescent staining of BmRpd3 (**A''**) at 24 h after 20E treatment in the fat body. Quantification of fluorescent BmRpd3 in the nucleus and cytoplasm in **A''** (**A'''**). N: nucleus, C: cytoplasm. (**B-B'''**) mRNA levels of *BmE75a* (**B**); protein levels of BmSqstm1, BmRpd3-HA, and BmAtg8 (**B'**); subcellular localization of the overexpressed BmRpd3-HA at 6 h after 20E treatment in BmN cells (**B''**). Quantification of fluorescent BmRpd3-HA in **B''** (**B'''**). (**C-C'''**) mRNA levels of *BmUsp* (**C**); protein levels of BmSqstm1, BmRpd3, and BmAtg8 (**C'**); immunofluorescent staining of BmRpd3 (**C''**) at 24 h after *BmUsp* RNAi in the fat body. Quantification of fluorescent BmRpd3 in **C''** (**C'''**).

Figure 5. Phosphorylation levels and subcellular localization of BmRpd3 after its phosphorylation sites mutation, 20E treatment, and MTORC1 inhibition in BmN cells. (**A**) Phosphorylation levels of BmRpd3-HA with a mutation at S392A (Ser392 to Ala392), S421A (Ser421 to Ala421), S423A (Ser423 to Ala423), or 3SA under normal feeding condition, 3SA: triple phosphorylation-site mutation, IP: immunoprecipitation. (**B-B'**) Subcellular localization of BmRpd3-HA with a mutation at S392A, S421A, S423A, or 3SA under normal feeding condition (**B**). Quantification of fluorescent BmRpd3-HA in the nucleus and cytoplasm in **B** (**B'**), N: nucleus, C: cytoplasm. (**C**) BmRpd3-HA protein levels in the nuclear and cytoplasmic proteins after the triple phosphorylation-site mutation, LMNB and TUBA1A are respectively used as nuclear and cytoplasmic reference proteins. (**D**) BmRpd3-HA phosphorylation levels after 20E treatment for 6 h; IgG immunoprecipitation is used as the negative control. (**E**) BmRpd3-HA protein levels in the nuclear and cytoplasmic proteins after 20E treatment for 6 h. (**F-G'**) Phosphorylation levels (**F**), and immunofluorescent staining

of BmRpd3-HA (**G**) after 20E, metformin, rapamycin, or compound C treatment for 6 h. Quantification of fluorescent BmRpd3-HA in the nucleus and cytoplasm in **G** (**G'**).

Figure 6. Mutation of S392, S421, and S423 in BmRpd3 promotes autophagy. (**A-B'**) Protein levels of BmSqstm1, EGFP-BmAtg8, and BmRpd3-HA (**A**), and fluorescent observation of EGFP-BmAtg8 and BmRpd3-HA, $BmRpd3^{S392A}$-HA, $BmRpd3^{S421A}$-HA, $BmRpd3^{S423A}$-HA or $BmRpd3^{3SA}$-HA after their respective co-overexpression with *egfp-BmAtg8* followed by 20E treatment for 6 h (**B**), quantification of EGFP-BmAtg8 puncta in **B** (**B'**), *mCherry* overexpression is used as the control. E-BmAtg8: EGFP-BmAtg8.

Figure 7. Cholesterol derivatives cooperate with nutrient signaling to regulate phosphorylation modification of BmRpd3. (**A-C'**) Protein levels of p-EIF4EBP1 after 20E (**A**), cholesterol (**B**) or 27-OH (**C**) treatment for 6 h. Quantification of p-EIF4EBP1, respectively in **A** (**A'**), **B** (**B'**), and **C** (**C'**). (**D-F**) mRNA level of *BmMTORC1* (**D**), phosphorylation levels of immunoprecipitated BmRpd3-HA (**E**), and immunofluorescent staining of BmRpd3-HA (**F**) after *BmMTORC1* RNAi treatment for 48 h in BmN cells.

Figure 8. Cholesterol derivatives induce dephosphorylation and cytoplasmic localization of HsHDAC1, and autophagy in HEK 293 cells. (**A-A"**) Protein levels of SQSTM1/p62 and LC3 after *HsHDAC1* overexpression or *HsHDAC1* overexpression followed by 40 μM CQ treatment (**A**). Punctation of EGFP-LC3 after *HsHDAC1* overexpression (**A'**). Quantification of EGFP-LC3 puncta in **A'** (**A"**). (**B-B"**) Protein levels of SQSTM1/p62, HsHDAC1-HA, and LC3 after 250 μM cholesterol treatment for 6 h, or 3 h followed by 40 μM CQ treatment for further 3 h (**B**); phosphorylation levels of immunoprecipitated HsHDAC1-HA (**B'**), and immunofluorescent staining of HsHDAC1 at 6 h after 250 μM cholesterol treatment (**B"**). (**C-C"**) Protein levels of SQSTM1/p62, HsHDAC1-HA, and LC3 after 5 μM 20E treatment for 6 h, or 3 h followed by 40 μM CQ treatment for further 3 h (**C**); phosphorylation levels of

immunoprecipitated HsHDAC1-HA (**C'**), and immunofluorescent staining of HsHDAC1 after 5 μM 20E treatment for 6 h (**C"**). (**D-D"**) Protein levels of SQSTM1/p62, HsHDAC1-HA, and LC3 after 10 μM 27-OH treatment for 6 h, or 3 h followed by 40 μM CQ treatment for further 3 h (**D**); phosphorylation levels of immunoprecipitated HsHDAC1-HA (**D'**), and immunofluorescent staining of HsHDAC1 after 10 μM 27-OH treatment for 6 h (**D"**).

Figure 9. BmRpd3 phosphorylation sites are functionally conserved and regulate phosphorylation levels, subcellular localization of HsHDAC1, and autophagy in HEK 293 cells. (**A-A"**) Phosphorylation levels (**A**) and immunofluorescent staining (**A'**) of HsHDAC1-HA mutated with a single phosphorylation site at S392A (Ser392 to Ala392), S421A (Ser421 to Ala421) or S423A (Ser423 to Ala423), or mutated with triple phosphorylation sites (3SA) under normal feeding condition. Quantification of fluorescent HsHDAC1-HA in the nucleus and the cytoplasm in **A'** (**A"**). (**B-B'**) Protein levels of SQSTM1/p62, HsHDAC1-HA, and LC3 after the overexpression of single or triple phosphorylation-site mutation of *HsHDAC1-HA* under normal feeding condition or or further treated with 27-OH, ACTB is used as the reference protein (**B**). Quantification of LC3-II in **B** (**B'**). (**C-C"**). Phosphorylation levels (**C**) and immunofluorescent staining (**C'**) of HsHDAC1-HA after 27-OH, metformin, rapamycin or compound C treatment for 6 h. Quantification of fluorescent HsHDAC1-HA in the nucleus (N) and cytoplasm (C) in **C'** (**C"**).

Figure 10. HsMTORC1 mediates the phosphorylation of HsHDAC1. (**A-A'**) p-EIF4EBP1 levels after cholesterol treatment for 6 h (**A**). Quantification of p-EIF4EBP1 in **A** (**A'**). (**B-B'**) p-EIF4EBP1 levels after 20E treatment for 6 h (**B**). Quantification of p-EIF4EBP1 in **B** (**B'**). (**C-C'**) p-EIF4EBP1 levels after 27-OH treatment for 6 h (**C**). Quantification of p-EIF4EBP1 in **C** (**C'**). (**D-F**) mRNA level of *HsMTORC1* (**D**), phosphorylation levels of immunoprecipitated HsHDAC1-HA (**E**), and immunofluorescent staining of HsHDAC1-HA (**F**) after *HsMTORC1* RNAi treatment for 48 h in HEK 293 cells.

Figure 11. A model for cholesterol derivatives in regulating BmRpd3/HsHDAC1 dephosphorylation and subsequent autophagy occurrence. MTORC1 signaling phosphorylates BmRpd3/HsHDAC1 and sequesters them in the nucleus. After being dephosphorylated by cholesterol derivatives signaling through inhibiting MTORC1 activity, BmRpd3/HsHDAC1 shuttles from the nucleus to the cytoplasm and promotes autophagy.

Figure S1. Prediction of binding between BmRpd3/HsHDAC1 and cholesterol derivatives. (**A-A"**) Three-dimensional structure models of BmRpd3 binding with 20E (**A**), 27-OH (**A'**), or cholesterol (**A"**). (**B-B"**) Three-dimensional structure models of HsHDAC1 binding with 20E (**B**), 27-OH (**B'**), or cholesterol (**B"**).

Figure S2. Quantification of BmAtg8–PE, SUMOylation level of BmRpd3 after 20E treatment, and BmRpd3 protein level after chemical treatments. (**A-C**) Quantification of BmAtg8–PE in **Fig. 4A'** (**A**); quantification of BmAtg8–PE in **Fig. 4B'** (**B**); quantification of BmAtg8–PE in **Fig. 4C'** (**C**). (**D**) SUMOylation levels of immunoprecipitated BmRpd3 after 20E treatment for 6 h in BmN cells. (**E-F**) Protein levels (**E**), and immunofluorescent staining (**F**) of BmRpd3 at 24 h after 20E, metformin, rapamycin or compound C treatment in *Bombyx* fat body. (**G**) Quantification of EGFP-BmAtg8–PE in **Fig. 6A**.

Figure S3. Cholesterol induces the cytoplasmic localization of BmRpd3 and autophagy in *B. mori*. (**A-A'**) Protein levels of BmSqstm1, BmRpd3, and BmAtg8 after 8 μg/larva cholesterol treatment for 24 h in the *B. mori* fat body (**A**). Quantification of BmAtg8–PE (columns) in **A**; quantification of nuclear and cytoplasmic BmRpd3 (line chart) in **B** at 24 h (**A'**). N: nucleus, C: cytoplasm. (**B**) Immunofluorescent staining of BmRpd3 after 8 μg/larva cholesterol treatment for 12 h and 24 h. (**C-C'**) Protein levels of BmSqstm1, BmRpd3, and BmAtg8 after *BmRpd3-HA* overexpression followed by different dose cholesterol treatment for 6 h

in BmN cells (**C**); quantification of BmAtg8–PE in **C** (**C'**), the control cells are treated with 500 μM cholesterol after *egfp* overexpression. (**D-D'**) Immunofluorescent staining of BmRpd3-HA at 6 h after different dose cholesterol treatment (**D**); quantification of BmRpd3-HA in the nucleus and the cytoplasm in **D** (**D'**). (**E**) Phosphorylation level of immunoprecipitated BmRpd3-HA at 6 h after 250 μM cholesterol treatment; IgG immunoprecipitation is used as the negative control.

Figure S4. Identification of phosphorylation sites in BmRpd3-HA and detection after CQ treatment. (**A-A"**) Immunoprecipitated BmRpd3-HA from BmN cells was separated by SDS-PAGE and further stained with Coomassie brilliant blue (**A**). Western blots of BmRpd3-HA using anti-HA tag antibody (**A'**), and an anti-phosphorylation antibody (**A"**); IgG immunoprecipitation is used as a negative control. (**B**) LC-MS/MS identification of the phosphorylation sites at Ser392, Ser421, and Ser423 in BmRpd3. (**C**) Alignment of the three phosphorylation sites in BmRpd3 with the homologs from *H. sapiens*, *M. musculus*, *D.melanogaster*, *S.litura*, *C. elegans,* and *S. cerevisiae*. (**D-D'**) Protein levels of SQSTM1/p62 and LC3 after 20, 40, 60, and 80 μM CQ treatments for 3 h in HEK 293 cells (**D**); quantification of LC3-II in **D** (**D'**).

Figure S5. Quantification of LC3-II protein and fluorescent HsHDAC1 after cholesterol derivative treatments, and subcellular localization of mCherry-LC3 after 27-OH treatment. (**A-G**) Quantification of LC3-II in **Fig. 8A** (**A**), **8B** (**B**), **8C** (**D**) and **8D** (**F**); quantification of fluorescent HsHDAC1 in the nucleus and the cytoplasm in **Fig. 8B"** (**C**), **8C"** (**E**), and **8D"** (**G**). (**H-H'**) Fluorescent observation of mCherry-LC3 co-overexpressed with *egfp*, *HsHDAC1-HA* or *HsHDAC1*^{3SA}*-HA* followed by 10 μM 27-OH treatment (**H**). Quantification of mCherry-LC3 puncta in **H** (**H'**).

Table S1. Predicted SUMOylation sites in BmRpd3.

Table S2. Primers for qPCR and RNAi.

Figure 1

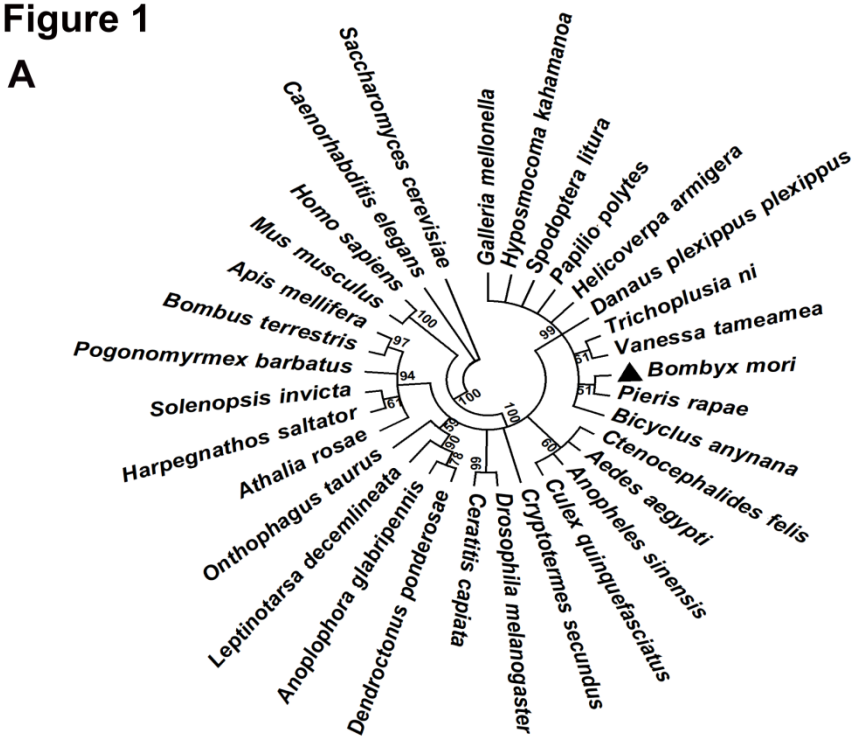

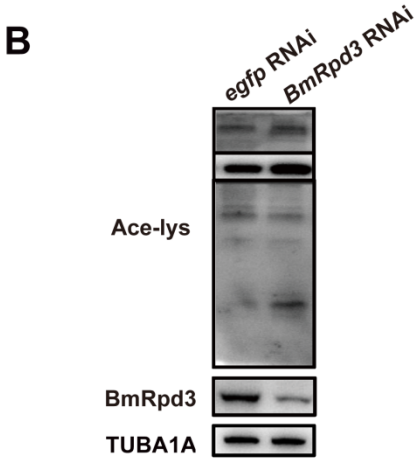

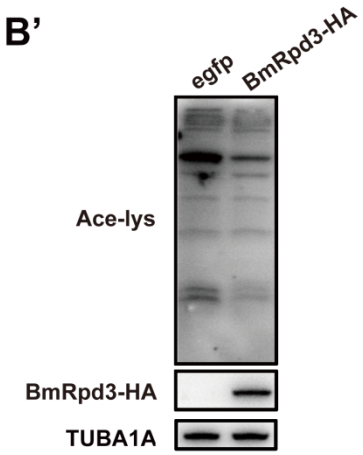

Figure 2

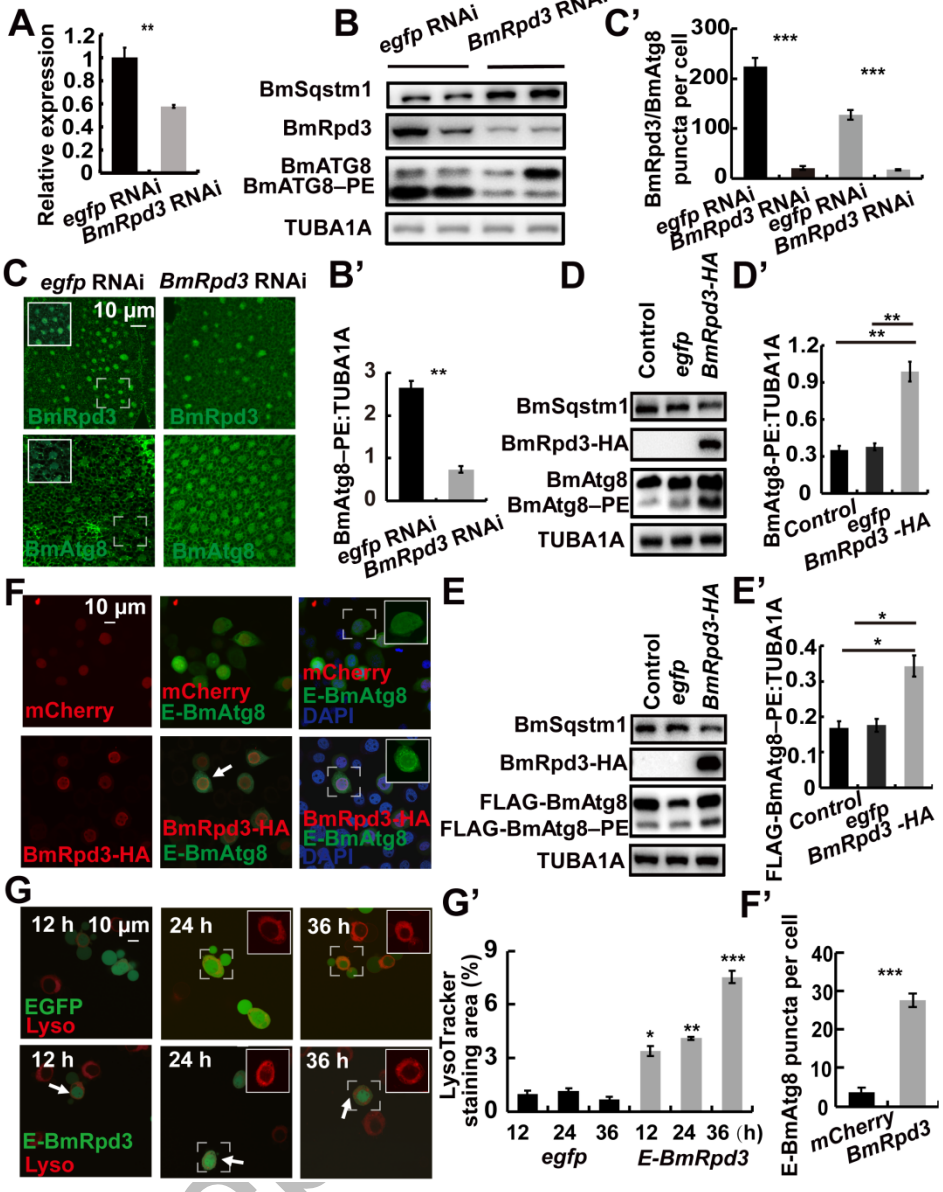

Figure 3

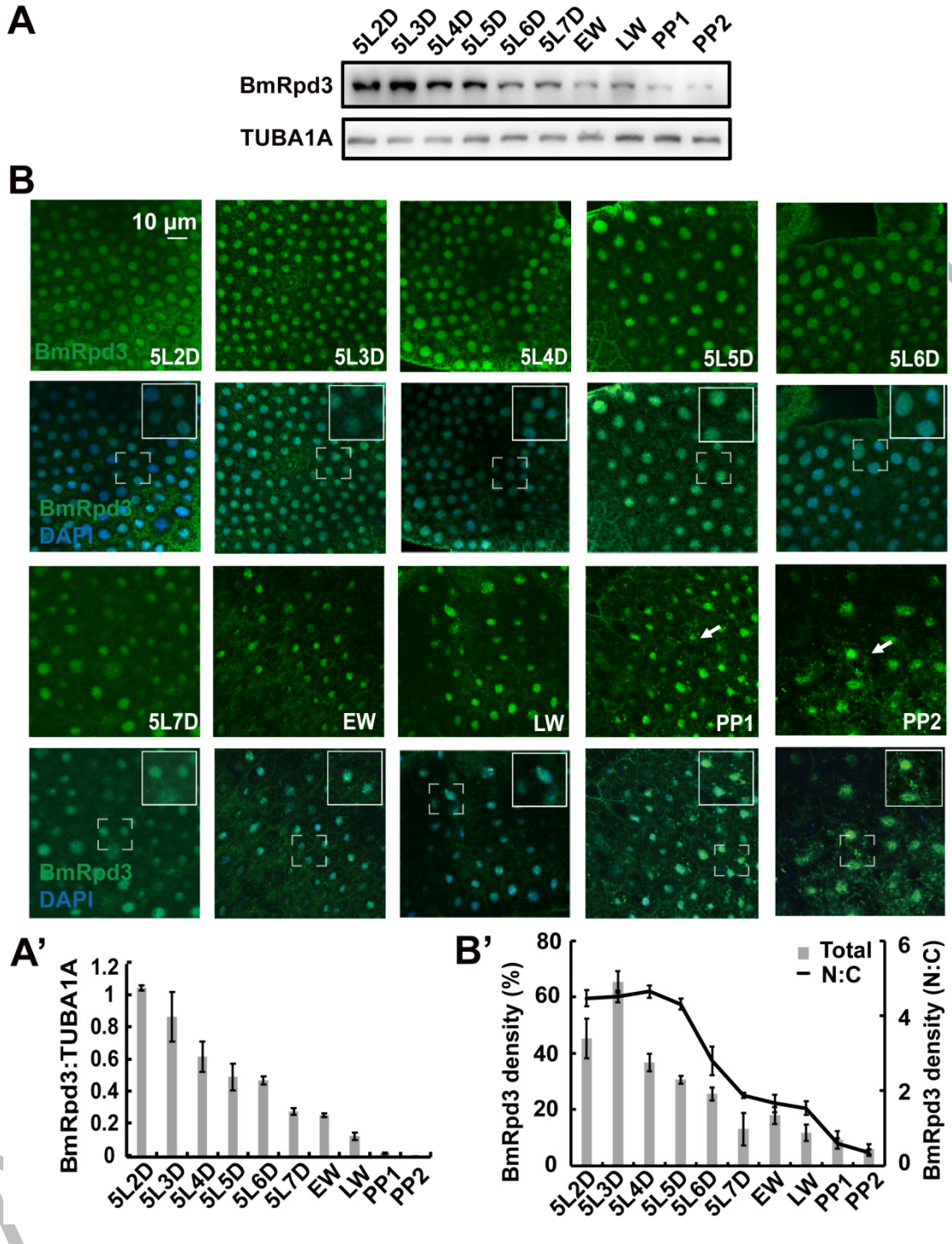
A
5L2D
5L3D
5L4D
5L5D
5L6D
5L7D
EW
LW
PP1
PP2
BmRpd3
TUBA1A
B
10 μm
BmRpd3
5L2D
5L3D
5L4D
5L5D
5L6D
BmRpd3
DAPI
5L7D
EW
LW
PP1
PP2
BmRpd3
DAPI
A'
BmRpd3:TUBA1A
1.2
1
0.8
0.6
0.4
0.2
0
5L2D
5L3D
5L4D
5L5D
5L6D
5L7D
EW
LW
PP1
PP2
B'
BmRpd3 density (%)
80
60
40
20
0
Total
N:C
6
4
2
0
BmRpd3 density (N:C)
5L2D
5L3D
5L4D
5L5D
5L6D
5L7D
EW
LW
PP1
PP2

Figure 4

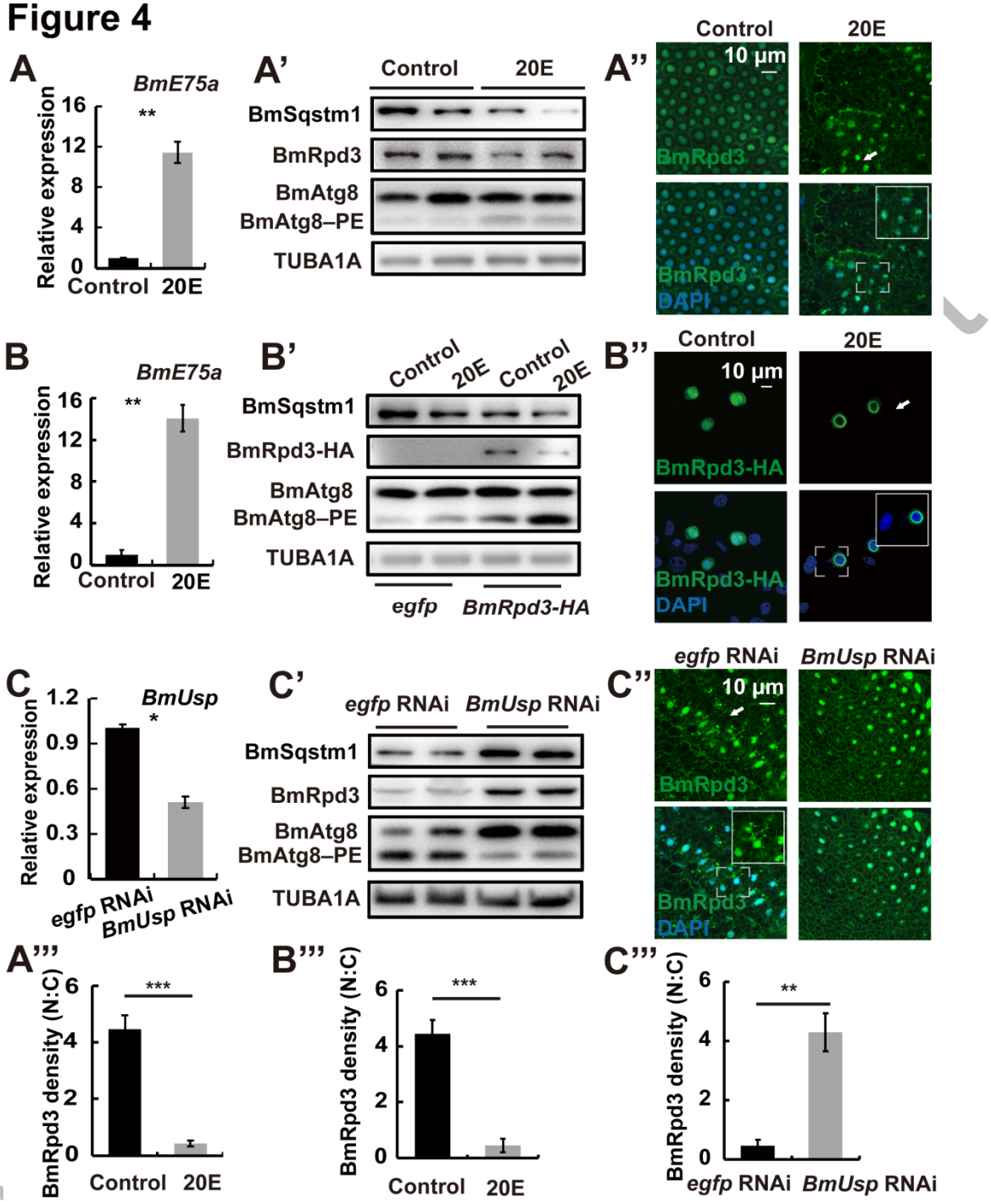
A
BmE75a
Relative expression
16
12
8
4
0
**
Control
20E
A'
Control
20E
BmSqstm1
BmRpd3
BmAtg8
BmAtg8–PE
TUBA1A
A''
Control
20E
10 μm
BmRpd3
BmRpd3
DAPI
B
BmE75a
Relative expression
16
12
8
4
0
**
Control
20E
B'
Control
20E
Control
20E
BmSqstm1
BmRpd3-HA
BmAtg8
BmAtg8–PE
TUBA1A
egfp
BmRpd3-HA
B''
Control
20E
10 μm
BmRpd3-HA
BmRpd3-HA
DAPI
C
BmUsp
Relative expression
1.2
0.9
0.6
0.3
0
*
egfp RNAi
BmUsp RNAi
C'
egfp RNAi
BmUsp RNAi
BmSqstm1
BmRpd3
BmAtg8
BmAtg8–PE
TUBA1A
C''
egfp RNAi
BmUsp RNAi
10 μm
BmRpd3
BmRpd3
DAPI
A'''
BmRpd3 density (N:C)
6
4
2
0
***
Control
20E
B'''
BmRpd3 density (N:C)
6
4
2
0
***
Control
20E
C'''
BmRpd3 density (N:C)
6
4
2
0
**
egfp RNAi
BmUsp RNAi

Figure 5

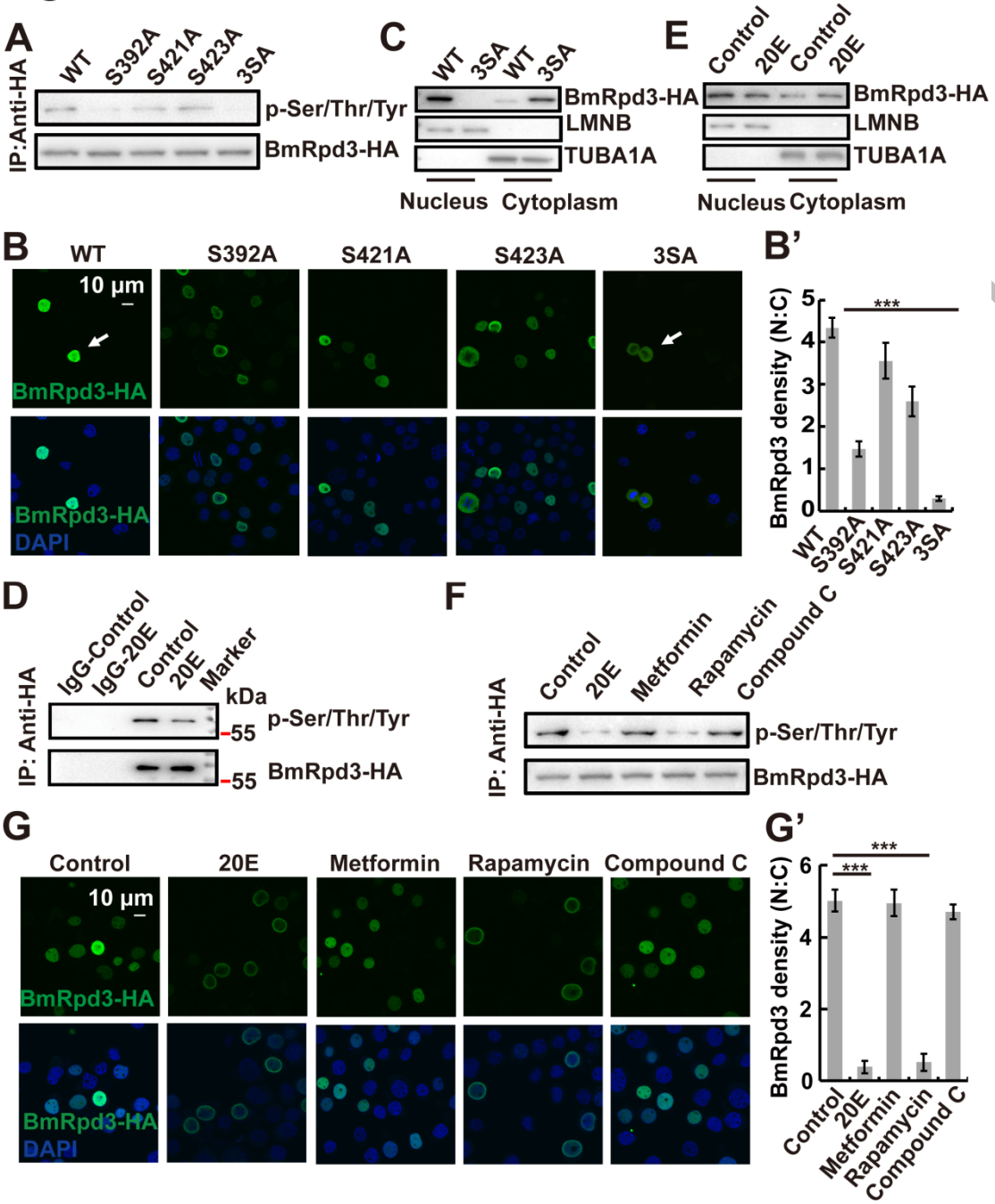
A
WT
S392A
S421A
S423A
3SA
IP:Anti-HA
p-Ser/Thr/Tyr
BmRpd3-HA
C
WT
3SA
WT
3SA
BmRpd3-HA
LMNB
TUBA1A
Nucleus
Cytoplasm
E
Control
20E
Control
20E
BmRpd3-HA
LMNB
TUBA1A
Nucleus
Cytoplasm
B
WT
S392A
S421A
S423A
3SA
10 μm
BmRpd3-HA
BmRpd3-HA
DAPI
B'
BmRpd3 density (N:C)
***
WT
S392A
S421A
S423A
3SA
D
IgG-Control
IgG-20E
Control
20E
Marker
kDa
IP: Anti-HA
55
p-Ser/Thr/Tyr
55
BmRpd3-HA
F
Control
20E
Metformin
Rapamycin
Compound C
IP: Anti-HA
p-Ser/Thr/Tyr
BmRpd3-HA
G
Control
20E
Metformin
Rapamycin
Compound C
10 μm
BmRpd3-HA
BmRpd3-HA
DAPI
G'
BmRpd3 density (N:C)
***
***
Control
20E
Metformin
Rapamycin
Compound C

Figure 6

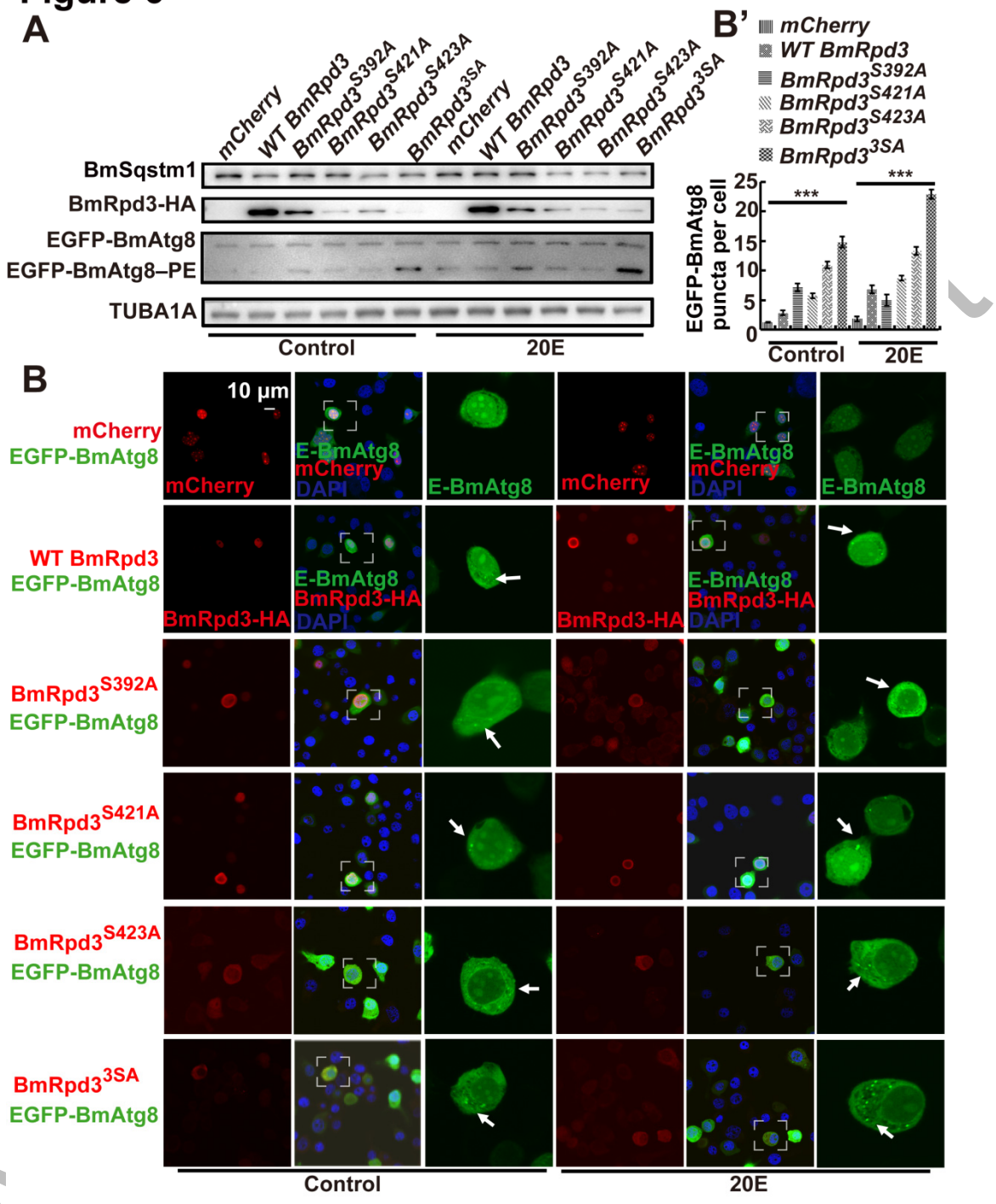
A
mCherry
WT BmRpd3
BmRpd3S392A
BmRpd3S421A
BmRpd3S423A
BmRpd3 3SA
BmSqstm1
BmRpd3-HA
EGFP-BmAtg8
EGFP-BmAtg8–PE
TUBA1A
Control
20E
B'
mCherry
WT BmRpd3
BmRpd3S392A
BmRpd3S421A
BmRpd3S423A
BmRpd3 3SA
EGFP-BmAtg8 puncta per cell
***
***
Control
20E
B
10 μm
mCherry
EGFP-BmAtg8
E-BmAtg8
mCherry
DAPI
WT BmRpd3
BmRpd3-HA
BmRpd3S392A
BmRpd3S421A
BmRpd3S423A
BmRpd3 3SA
Control
20E

Figure 7

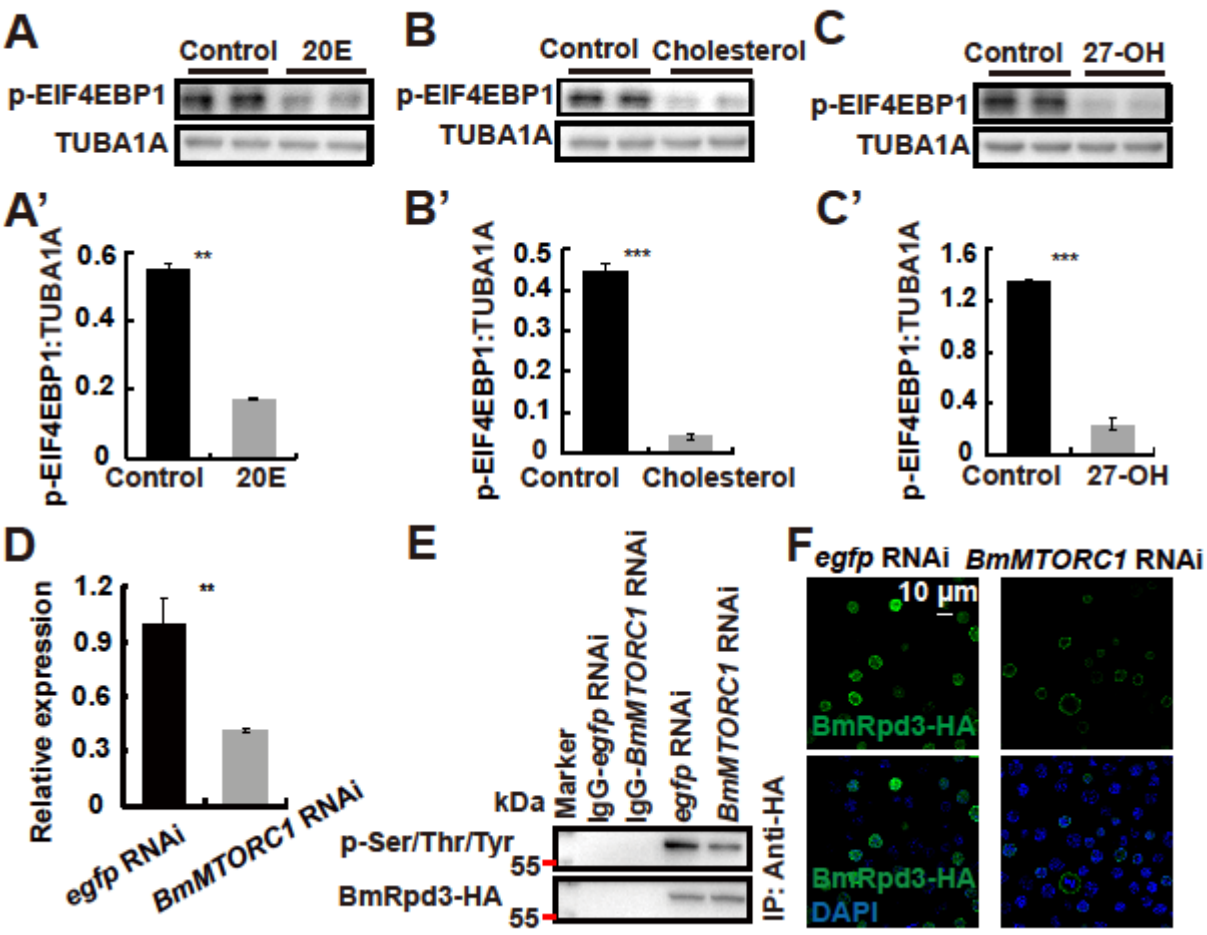
A
Control
20E
p-EIF4EBP1
TUBA1A
B
Control
Cholesterol
p-EIF4EBP1
TUBA1A
C
Control
27-OH
p-EIF4EBP1
TUBA1A
A'
p-EIF4EBP1:TUBA1A
0.6
0.4
0.2
0
**
Control
20E
B'
p-EIF4EBP1:TUBA1A
0.5
0.4
0.3
0.2
0.1
0
***
Control
Cholesterol
C'
p-EIF4EBP1:TUBA1A
1.6
1.2
0.8
0.4
0
***
Control
27-OH
D
Relative expression
1.2
0.9
0.6
0.3
0
**
egfp RNAi
BmMTORC1 RNAi
E
kDa
Marker
IgG-egfp RNAi
IgG-BmMTORC1 RNAi
egfp RNAi
BmMTORC1 RNAi
p-Ser/Thr/Tyr
55
BmRpd3-HA
55
IP: Anti-HA
F
egfp RNAi
BmMTORC1 RNAi
10 μm
BmRpd3-HA
BmRpd3-HA
DAPI

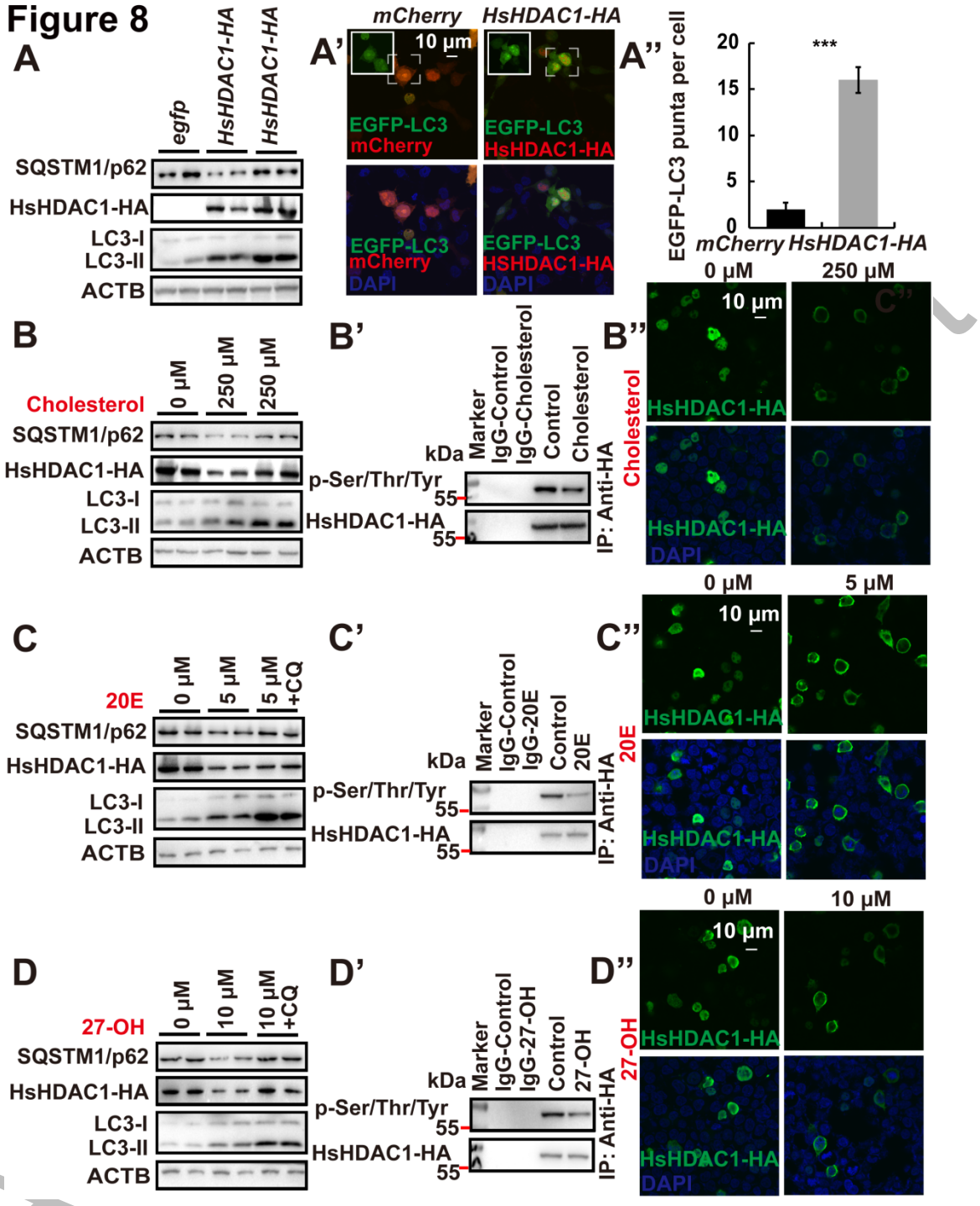
Figure 8
A
egfp
HsHDAC1-HA
HsHDAC1-HA
SQSTM1/p62
HsHDAC1-HA
LC3-I
LC3-II
ACTB
A'
mCherry
HsHDAC1-HA
10 μm
EGFP-LC3
mCherry
EGFP-LC3
HsHDAC1-HA
EGFP-LC3
mCherry
DAPI
EGFP-LC3
HSHDAC1-HA
DAPI
A''
EGFP-LC3 punta per cell
20
15
10
5
0
***
mCherry
HsHDAC1-HA
B
Cholesterol
0 μM
250 μM
250 μM
SQSTM1/p62
HsHDAC1-HA
LC3-I
LC3-II
ACTB
B'
kDa
Marker
IgG-Control
IgG-Cholesterol
Control
Cholesterol
p-Ser/Thr/Tyr
55
HsHDAC1-HA
55
IP: Anti-HA
B''
0 μM
250 μM
10 μm
Cholesterol
HsHDAC1-HA
HsHDAC1-HA
DAPI
C
20E
0 μM
5 μM
5 μM
+CQ
SQSTM1/p62
HsHDAC1-HA
LC3-I
LC3-II
ACTB
C'
kDa
Marker
IgG-Control
IgG-20E
Control
20E
p-Ser/Thr/Tyr
55
HsHDAC1-HA
55
IP: Anti-HA
C''
0 μM
5 μM
10 μm
20E
HsHDAC1-HA
HsHDAC1-HA
DAPI
D
27-OH
0 μM
10 μM
10 μM
+CQ
SQSTM1/p62
HsHDAC1-HA
LC3-I
LC3-II
ACTB
D'
kDa
Marker
IgG-Control
IgG-27-OH
Control
27-OH
p-Ser/Thr/Tyr
55
HsHDAC1-HA
55
IP: Anti-HA
D''
0 μM
10 μM
10 μm
27-OH
HsHDAC1-HA
HsHDAC1-HA
DAPI

Figure 9

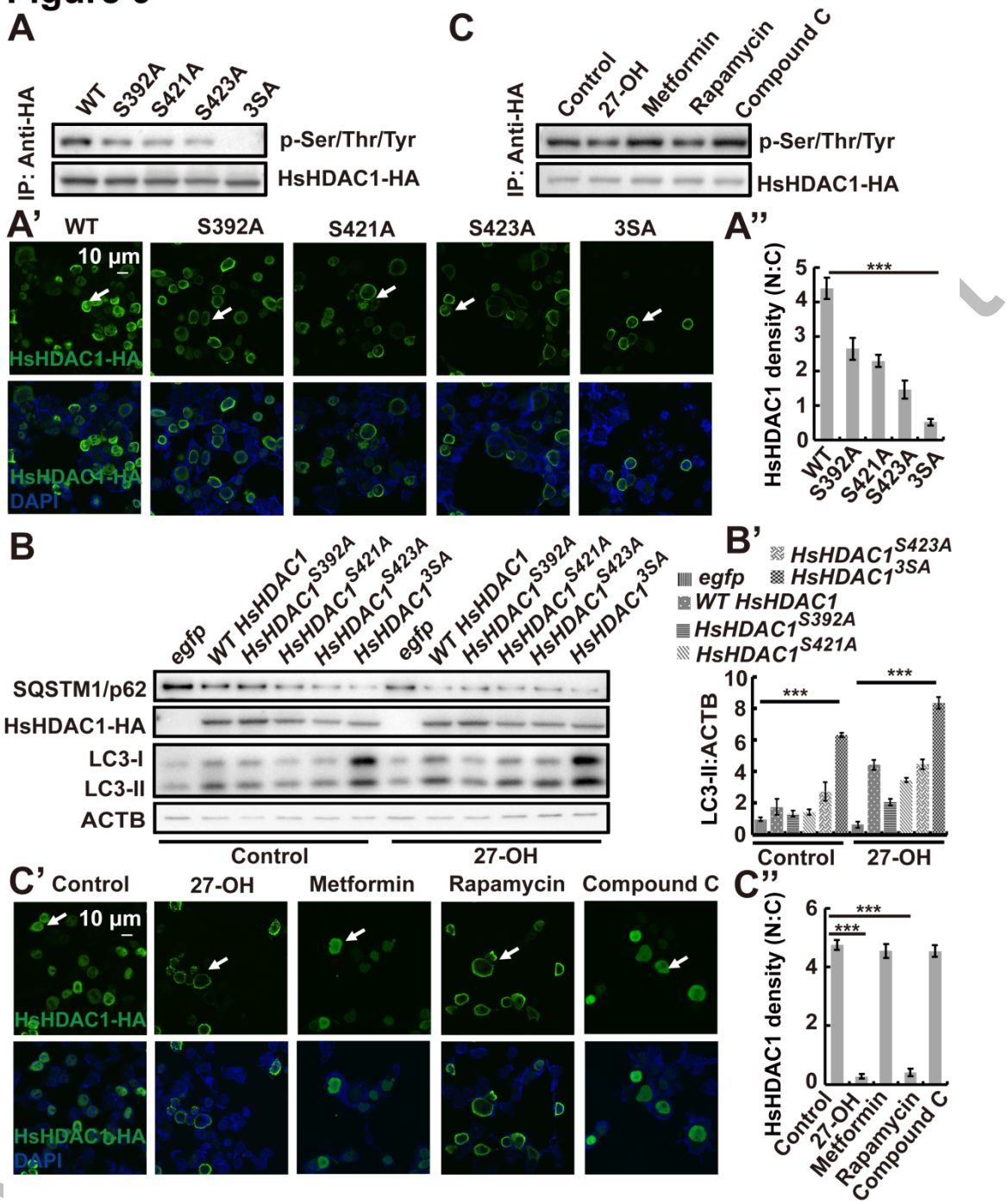
A
IP: Anti-HA
WT
S392A
S421A
S423A
3SA
p-Ser/Thr/Tyr
HsHDAC1-HA
C
IP: Anti-HA
Control
27-OH
Metformin
Rapamycin
Compound C
p-Ser/Thr/Tyr
HsHDAC1-HA
A'
WT
S392A
S421A
S423A
3SA
10 μm
HsHDAC1-HA
HsHDAC1-HA
DAPI
A''
HsHDAC1 density (N:C)
***
WT
S392A
S421A
S423A
3SA
B
egfp
WT HsHDAC1
HsHDAC1S392A
HsHDAC1S421A
HsHDAC1S423A
HsHDAC13SA
SQSTM1/p62
HsHDAC1-HA
LC3-I
LC3-II
ACTB
Control
27-OH
B'
HsHDAC1S423A
HsHDAC13SA
egfp
WT HsHDAC1
HsHDAC1S392A
HsHDAC1S421A
LC3-II:ACTB
***
***
Control
27-OH
C' Control
27-OH
Metformin
Rapamycin
Compound C
10 μm
HsHDAC1-HA
HsHDAC1-HA
DAPI
C''
HsHDAC1 density (N:C)
***
***
Control
27-OH
Metformin
Rapamycin
Compound C

Figure 10

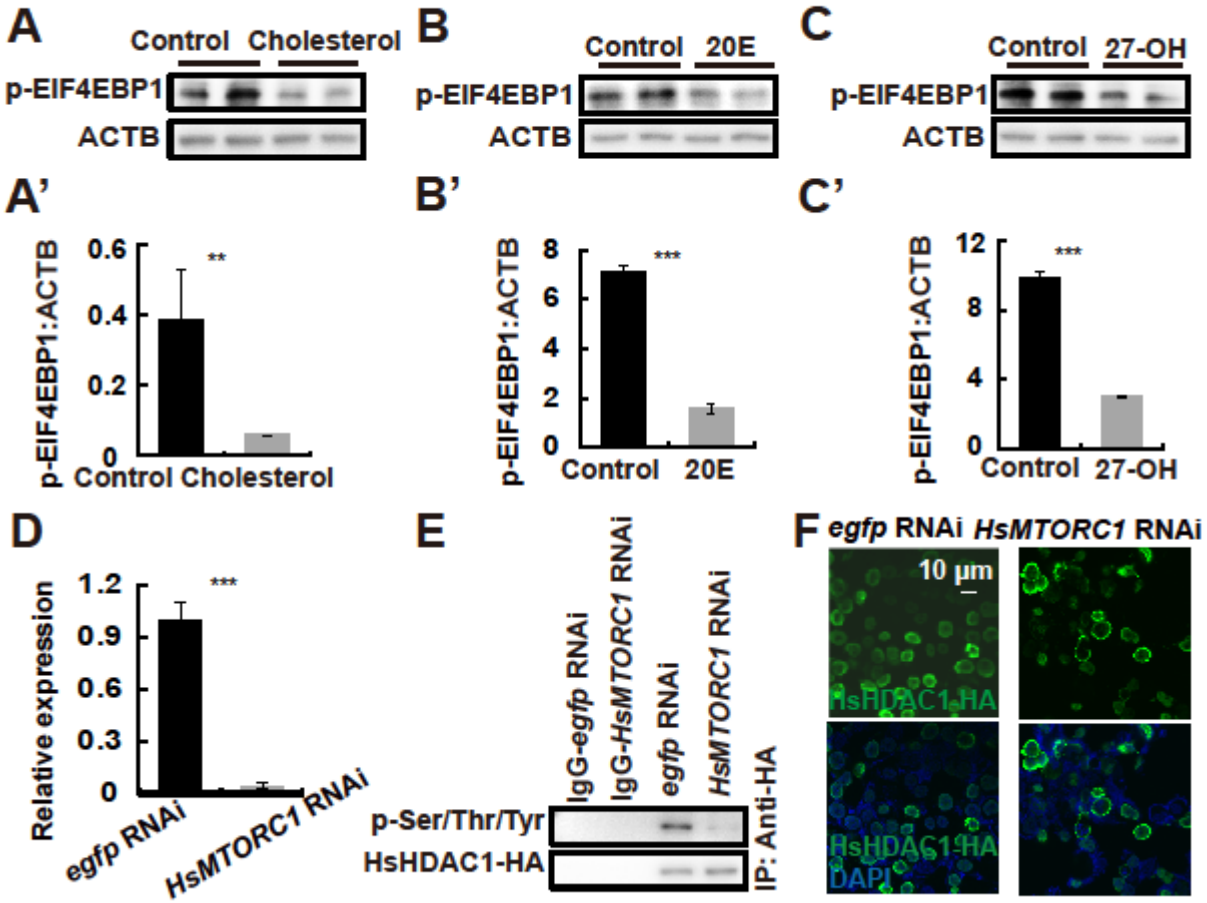
A
Control
Cholesterol
p-EIF4EBP1
ACTB
B
Control
20E
p-EIF4EBP1
ACTB
C
Control
27-OH
p-EIF4EBP1
ACTB
A'
p-EIF4EBP1:ACTB
0.6
0.4
0.2
0
**
Control
Cholesterol
B'
p-EIF4EBP1:ACTB
8
6
4
2
0
***
Control
20E
C'
p-EIF4EBP1:ACTB
12
8
4
0
***
Control
27-OH
D
Relative expression
1.2
0.9
0.6
0.3
0
***
egfp RNAi
HsMTORC1 RNAi
E
IgG-egfp RNAi
IgG-HsMTORC1 RNAi
egfp RNAi
HsMTORC1 RNAi
p-Ser/Thr/Tyr
HsHDAC1-HA
IP: Anti-HA
F
egfp RNAi
HsMTORC1 RNAi
10 μm
HsHDAC1-HA
HsHDAC1-HA
DAPI

Figure 11

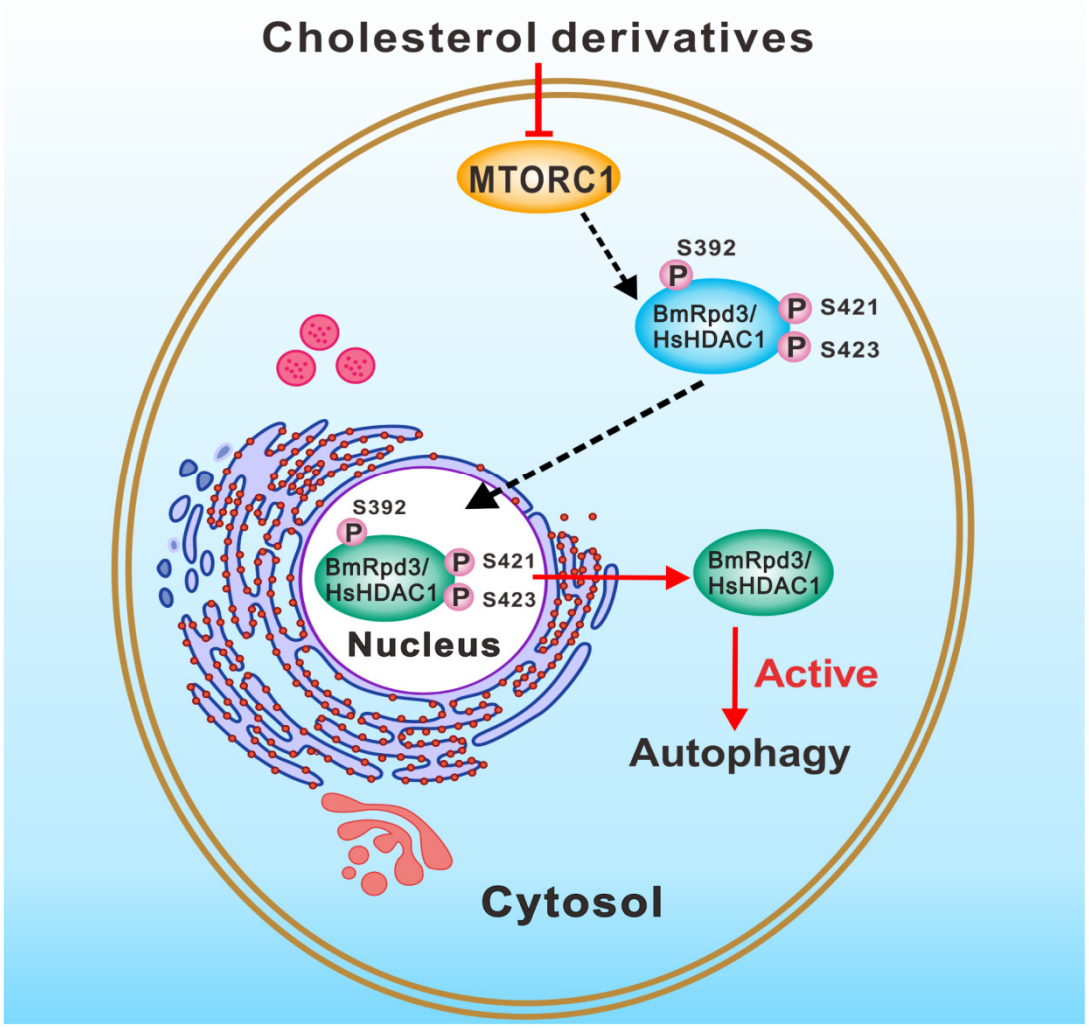

Figure S1

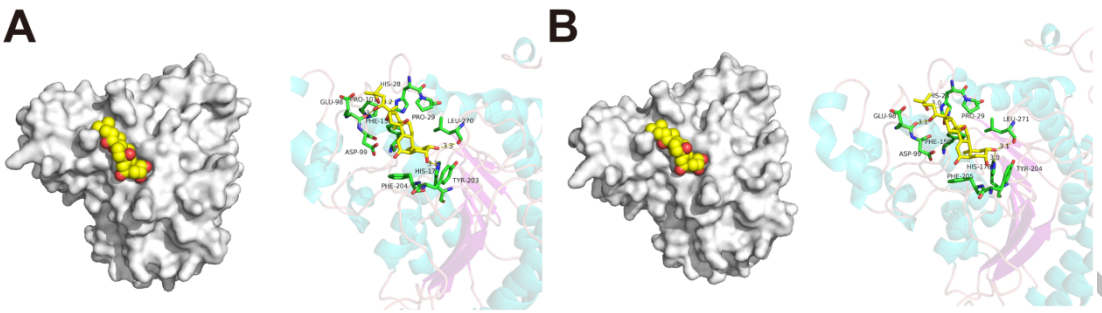

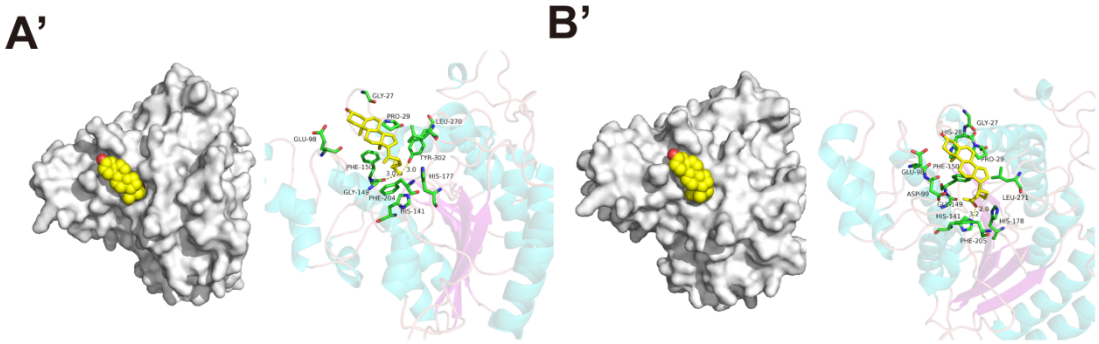

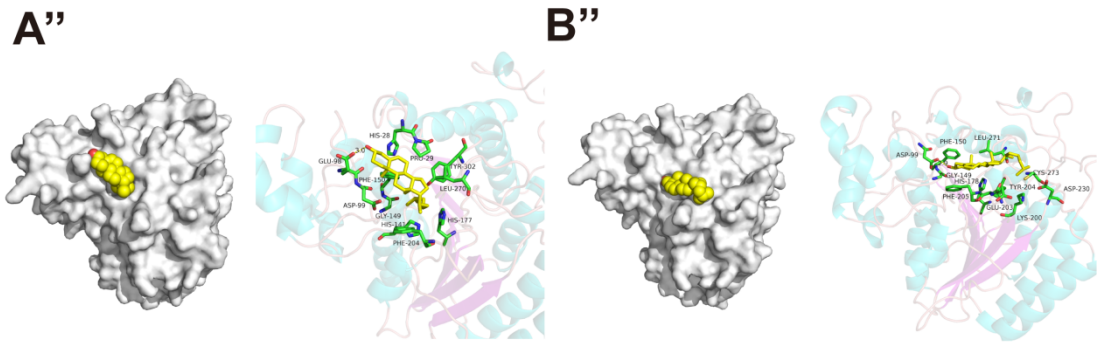

Figure S2

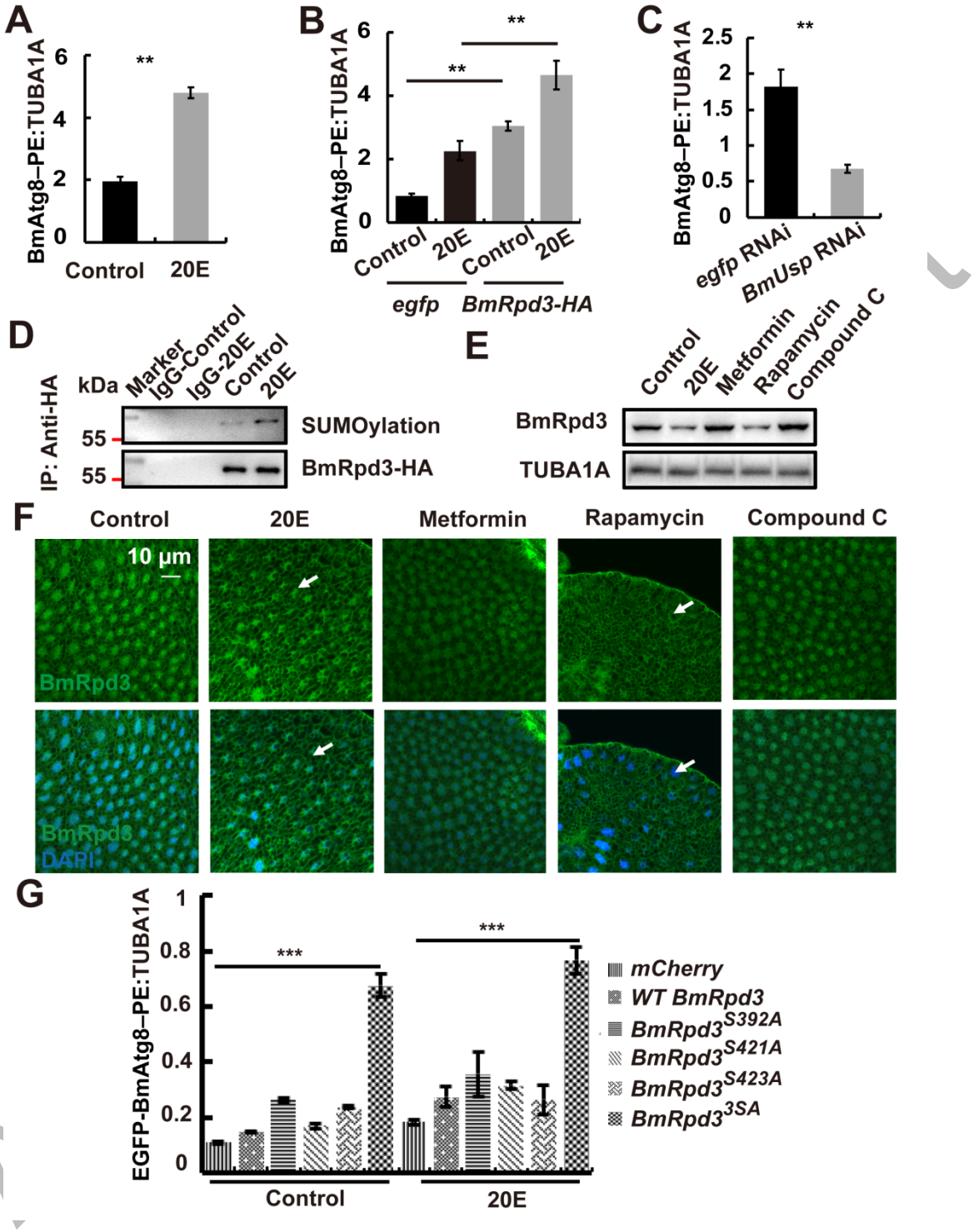
A
BmAtg8–PE:TUBA1A
Control
20E
B
BmAtg8–PE:TUBA1A
Control
20E
Control
20E
egfp
BmRpd3-HA
C
BmAtg8–PE:TUBA1A
egfp RNAi
BmUsp RNAi
D
IP: Anti-HA
kDa
Marker
IgG-Control
IgG-20E
Control
20E
55
55
SUMOylation
BmRpd3-HA
E
Control
20E
Metformin
Rapamycin
Compound C
BmRpd3
TUBA1A
F
Control
20E
Metformin
Rapamycin
Compound C
10 μm
BmRpd3
BmRpd3
DAPI
G
EGFP-BmAtg8–PE:TUBA1A
Control
20E
mCherry
WT BmRpd3
BmRpd3S392A
BmRpd3S421A
BmRpd3S423A
BmRpd33SA

Figure S3

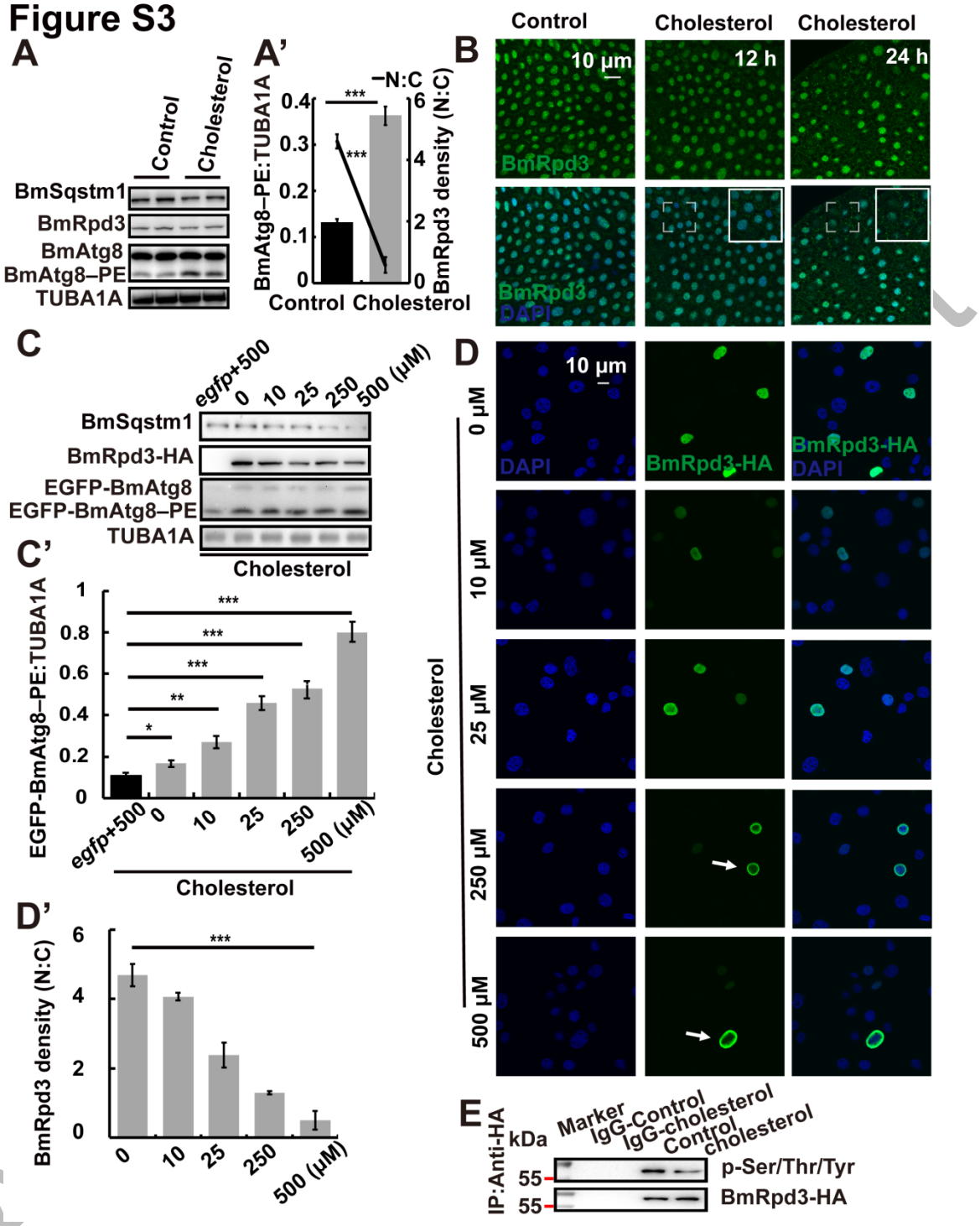
A
Control
Cholesterol
BmSqstm1
BmRpd3
BmAtg8
BmAtg8–PE
TUBA1A
A'
BmAtg8–PE:TUBA1A
N:C
BmRpd3 density (N:C)
Control
Cholesterol
B
Control
Cholesterol
Cholesterol
10 μm
12 h
24 h
BmRpd3
BmRpd3
DAPI
C
egfp+500
0
10
25
250
500 (μM)
BmSqstm1
BmRpd3-HA
EGFP-BmAtg8
EGFP-BmAtg8–PE
TUBA1A
Cholesterol
C'
EGFP-BmAtg8–PE:TUBA1A
Cholesterol
D
10 μm
DAPI
BmRpd3-HA
BmRpd3-HA
DAPI
0 μM
10 μM
25 μM
250 μM
500 μM
Cholesterol
D'
BmRpd3 density (N:C)
0
10
25
250
500 (μM)
E
IP:Anti-HA
kDa
Marker
IgG-Control
IgG-cholesterol
Control
cholesterol
55
55
p-Ser/Thr/Tyr
BmRpd3-HA

Figure S4

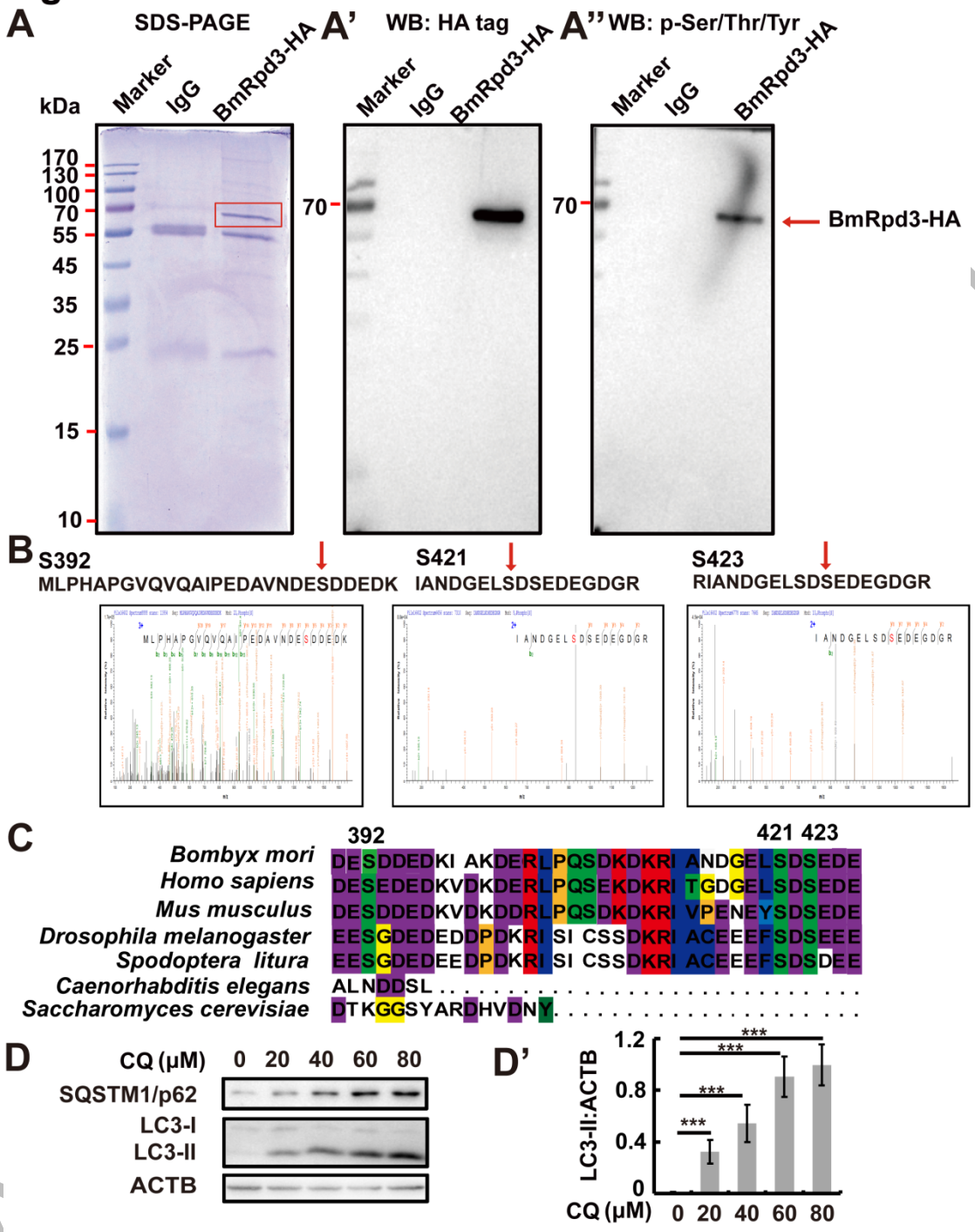
A
SDS-PAGE
A'
WB: HA tag
A''
WB: p-Ser/Thr/Tyr
Marker
IgG
BmRpd3-HA
kDa
170
130
100
70
55
45
35
25
15
10
70
70
BmRpd3-HA
B
S392
MLPHAPGVQVQAIPEDAVNDESDDEDK
S421
IANDGELSDSEDEGDGR
S423
RIANDGELSDSEDEGDGR
C
392
421 423
Bombyx mori
Homo sapiens
Mus musculus
Drosophila melanogaster
Spodoptera litura
Caenorhabditis elegans
Saccharomyces cerevisiae
D
CQ (μM)
0 20 40 60 80
SQSTM1/p62
LC3-I
LC3-II
ACTB
D'
LC3-II:ACTB
1.2
0.8
0.4
0
***
CQ (μM)
0 20 40 60 80

Figure S5

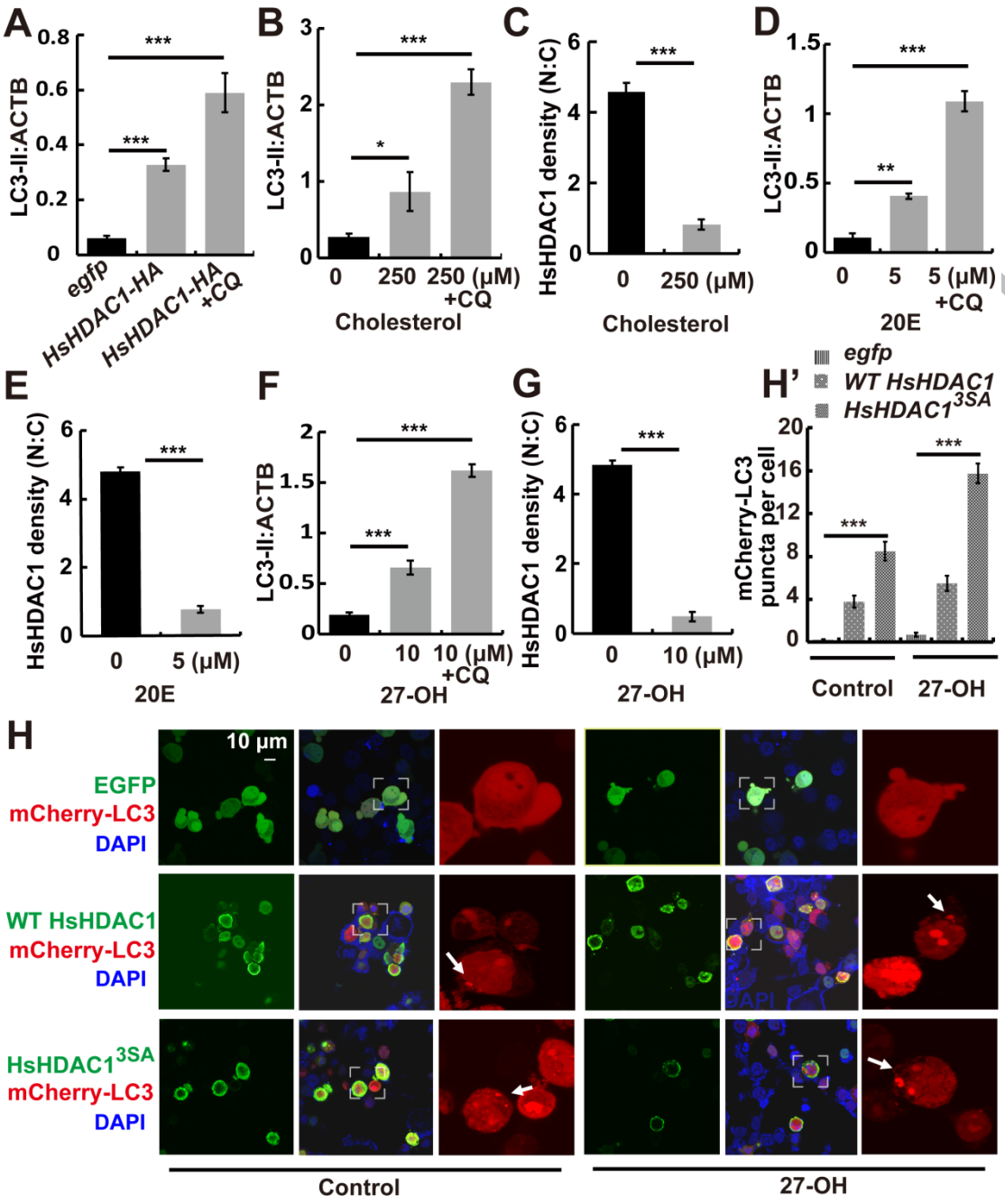
A
LC3-II:ACTB
egfp
HsHDAC1-HA
HsHDAC1-HA +CQ
B
LC3-II:ACTB
0
250
250 (μM) +CQ
Cholesterol
C
HsHDAC1 density (N:C)
0
250 (μM)
Cholesterol
D
LC3-II:ACTB
0
5
5 (μM) +CQ
20E
E
HsHDAC1 density (N:C)
0
5 (μM)
20E
F
LC3-II:ACTB
0
10
10 (μM) +CQ
27-OH
G
HsHDAC1 density (N:C)
0
10 (μM)
27-OH
H'
egfp
WT HsHDAC1
HsHDAC1 3SA
mCherry-LC3 puncta per cell
Control
27-OH
H
10 μm
EGFP
mCherry-LC3
DAPI
WT HsHDAC1
mCherry-LC3
DAPI
HsHDAC1 3SA
mCherry-LC3
DAPI
Control
27-OH

ID	Position	Peptide	Score	Cutoff	P-Value
50	LNYGLYRKMBIYRPH	4.109	3.32	0.054	Sumoylation Nonconcensus
170-174	LLKYHQRVLYIDIDVHHGD	30.815	29.92	0.147	SUMO Interaction
398	DESDDEDKIAKDERL	3.364	3.32	0.12	Sumoylation Nonconcensus
454	DKEPLQIKDDLKPDD	3.518	2.13	0.037	Sumoylation Concensus
458	LQIKDDLKPDDMKDD	3.633	2.13	0.033	Sumoylation Concensus
463	DLKPDDMKDDVKNVS	6.363	2.13	0.027	Sumoylation Concensus
476	VSNAEESKKDMPPNP	9.655	3.32	0.039	Sumoylation Nonconcensus
477	SNAEESKKDMPPNP*	5.35	3.32	0.043	Sumoylation Nonconcensus

Table S1

Table S2 Primers of PCR

Gene name	Genbank number	Primer sequence
BmRpd3 F	XM_004931383.3	CATGCCATGGCAATGTCTATGCAACCGCACAGTAAGAAAAG
BmRpd3 R		TCAGGGATTCGGTGGCATGTCCTTCTTT
BmRpd3 HA R		CGGGGTACCTCAAGCGTAATCTGGAACATCGTATGGGTAGGGATTCGGTGGCATGTCCTTCTTT
BmAtg8 F	NM_001046779.1	ATGAAATTCCAATACAAAGAAG
BmAtg8 FLAG F		GGAAGATCTGACTACAAGGACGACGATGACAAGATGAAATTCCAATACAAAG
BmAtg8 R		CGGGGTACCTTAATTTCCATAGACATTTTCGTC
qPCR-*BmE75a* F	NP_001106079.1	CTTCGGCTCATGCACTCCTG
qPCR-*BmE75a* R		GTTCACGTTCCTTGTGCATCG
qPCR-*BmUsp* F	NM_001044005	TCAAATAGGCAACAAACAGA
qPCR-*BmUsp* R		CAGGAACTCCATAGACCG
qPCR-*BmRP49* F		CAGGCGGTTCAAGGGTCAATAC
qPCR-*BmRP49* R		TGCTGGGCTCTTTCCACGA
qPCR-*BmRpd3* F		AGCGTTGACATTGACAGA
qPCR-*BmRpd3* R		TGACGATGGTGAAGATGC
qPCR-*BmMTOR1*-F		GCCACCTCCAAGCTACCCTAATAATGTT

qPCR-*BmMTOR1*-R	AATCTATCCTTGCTTGTGTCGTGTTTC
qPCR-*HsMTOR1*-F	TCAGAATCCAAGTCAAGTCA
qPCR-*HsMTOR1*-R	CTCATCCAGAGGCAAGTT
qPCR-*ACTB*-F	TGGTGCGAATGGGTCAGAA
qPCR-*ACTB*-R	CCGCCAGAGGCATACAGG
BmRpd3 RNAi F	GGATCCTAATACGACTCACTATAGGATATTGACATAGATGTGCATCATGGTG
BmRpd3 RNAi R	GGATCCTAATACGACTCACTATAGGCGAGATACATTACGTATGGTATATCCGCCT
BmUsp RNAi F	GGATCCTAATACGACTCACTATAGGCCCTAACCATCCCTTGA
BmUsp RNAi R	GGATCCTAATACGACTCACTATAGGTGAATCCGCAACTAACG
egfp RNAi F	GGATCCTAATACGACTCACTATAGGGAGAATGGTGAGCAAGGGCG
egfp RNAi R	GGATCCTAATACGACTCACTATAGGGAGACTTGTACAGCTCGTCC
*BmMTOR1*si-F	UCGUAGAUAAUUUGCAUAGCG
*BmMTOR1*si-R	CUAUGCAAAUUAUCUACGAAA
egfp si-F	GGCUACGUCCAGGAGCGCACC
egfp si-R	UGCGCUCCUGGACGUAGCCUU
*HsMTOR1*si-F	GCUAAAGAAGGACAUUCAAGA
*HsMTOR1*si-R	UUGAAUGUCCUUCUUUAGCUG